

1 **A prefusion SARS-CoV-2 spike RNA vaccine is highly immunogenic and**  
2 **prevents lung infection in non-human primates**

3

4 **Authors**

5 Annette B. Vogel<sup>1#</sup>, Isis Kanevsky<sup>2#</sup>, Ye Che<sup>3</sup>, Kena A. Swanson<sup>2</sup>, Alexander Muik<sup>1</sup>, Mathias  
6 Vormehr<sup>1</sup>, Lena M. Kranz<sup>1</sup>, Kerstin C. Walzer<sup>1</sup>, Stephanie Hein<sup>1</sup>, Alptekin Güler<sup>1</sup>, Jakob  
7 Loschko<sup>2</sup>, Mohan S. Maddur<sup>2</sup>, Kristin Tompkins<sup>2</sup>, Journey Cole<sup>4</sup>, Bonny G. Lui<sup>1</sup>, Thomas  
8 Ziegenhals<sup>1</sup>, Arianne Plaschke<sup>1</sup>, David Eisel<sup>1</sup>, Sarah C. Dany<sup>1</sup>, Stephanie Fesser<sup>1</sup>, Stephanie  
9 Erbar<sup>1</sup>, Ferdia Bates<sup>1</sup>, Diana Schneider<sup>1</sup>, Bernadette Jesionek<sup>1</sup>, Bianca Sängler<sup>1</sup>, Ann-Kathrin  
10 Wallisch<sup>1</sup>, Yvonne Feuchter<sup>1</sup>, Hanna Junginger<sup>1</sup>, Stefanie A. Krumm<sup>1</sup>, André P. Heinen<sup>1</sup>, Petra  
11 Adams-Quack<sup>1</sup>, Julia Schlereth<sup>1</sup>, Christoph Kröner<sup>1</sup>, Shannan Hall-Ursone<sup>4</sup>, Kathleen Brasky<sup>4</sup>,  
12 Matthew C. Griffor<sup>3</sup>, Seungil Han<sup>3</sup>, Joshua A. Lees<sup>3</sup>, Ellene H. Mashalidis<sup>3</sup>, Parag V.  
13 Sahasrabudhe<sup>3</sup>, Charles Y. Tan<sup>2</sup>, Danka Pavliakova<sup>2</sup>, Guy Singh<sup>2</sup>, Camila Fontes-Garfias<sup>5</sup>,  
14 Michael Pride<sup>2</sup>, Ingrid L. Scully<sup>2</sup>, Tara Ciolino<sup>2</sup>, Jennifer Obregon<sup>2</sup>, Michal Gazi<sup>6</sup>, Ricardo  
15 Carrion, Jr.<sup>4</sup>, Kendra J. Alfson<sup>6</sup>, Warren V. Kalina<sup>2</sup>, Deepak Kaushal<sup>4</sup>, Pei-Yong Shi<sup>5</sup>, Thorsten  
16 Klamp<sup>1</sup>, Corinna Rosenbaum<sup>1</sup>, Andreas N. Kuhn<sup>1</sup>, Özlem Türeci<sup>1</sup>, Philip R. Dormitzer<sup>2</sup>,  
17 Kathrin U. Jansen<sup>2</sup>, Ugur Sahin<sup>1,7</sup>

18

19 # Contributed equally

20

21 **Affiliations:**

22 <sup>1</sup> BioNTech, An der Goldgrube 12, 55131 Mainz, Germany;

23 <sup>2</sup> Pfizer, 401 N. Middletown Rd., Pearl River, NY 10965, United States;

24 <sup>3</sup> Pfizer, 280 Shennecossett Rd., Groton, CT 06340, United States;

25 <sup>4</sup> Southwest National Primate Research Center, Texas Biomedical Research Institute, 8715 W.  
26 Military Dr, San Antonio, TX 78227, United States;

27 <sup>5</sup> University of Texas Medical Branch, 301 University Blvd, Galveston, TX 77555, United  
28 States;

29 <sup>6</sup> Texas Biomedical Research Institute, 8715 W Military Dr, San Antonio, TX 78227, United  
30 States;

31 <sup>7</sup> TRON gGmbH – Translational Oncology at the University Medical Center of the Johannes  
32 Gutenberg University, Freiligrathstraße 12, 55131 Mainz, Germany;

33

34 **Correspondence:** Prof. Dr. Ugur Sahin, BioNTech SE, An der Goldgrube 12, 55131 Mainz,  
35 Germany, Tel: +49 6131 2161 201; Email: [Ugur.Sahin@biontech.de](mailto:Ugur.Sahin@biontech.de)

## 36 **Abstract**

37 To contain the coronavirus disease 2019 (COVID-19) pandemic, a safe and effective vaccine  
38 against the new severe acute respiratory syndrome coronavirus-2 (SARS-CoV-2) is urgently  
39 needed in quantities sufficient to immunise large populations. In this study, we report the  
40 design, preclinical development, immunogenicity and anti-viral protective effect in rhesus  
41 macaques of the BNT162b2 vaccine candidate. BNT162b2 contains an LNP-formulated  
42 nucleoside-modified mRNA that encodes the spike glycoprotein captured in its prefusion  
43 conformation. After expression of the BNT162b2 coding sequence in cells, approximately 20%  
44 of the spike molecules are in the one-RBD ‘up’, two-RBD ‘down’ state. Immunisation of mice  
45 with a single dose of BNT162b2 induced dose level-dependent increases in pseudovirus  
46 neutralisation titers. Prime-boost vaccination of rhesus macaques elicited authentic SARS-  
47 CoV-2 neutralising geometric mean titers 10.2 to 18.0 times that of a SARS-CoV-2  
48 convalescent human serum panel. BNT162b2 generated strong  $T_H1$  type  $CD4^+$  and  $IFN\gamma^+$   $CD8^+$   
49 T-cell responses in mice and rhesus macaques. The BNT162b2 vaccine candidate fully  
50 protected the lungs of immunised rhesus macaques from infectious SARS-CoV-2 challenge.  
51 BNT162b2 is currently being evaluated in a global, pivotal Phase 2/3 trial (NCT04368728).

## 52 **Main**

### 53 **Introduction**

54 Due to the shattering impact of the coronavirus disease 2019 (COVID-19) pandemic on human  
55 health and society, multiple collaborative research programs have been launched, leading to  
56 new insights and progress towards vaccine development. Soon after it emerged in December  
57 2019, severe acute respiratory syndrome coronavirus-2 (SARS-CoV-2) was identified as a  $\beta$ -  
58 coronavirus with high sequence similarity to bat-derived SARS-like coronaviruses<sup>1,2</sup>. The  
59 globalised response is mirrored by the upload of over 92,000 viral genome sequences as of  
60 August 29, 2020, to GISAID (Global Initiative on Sharing All Influenza Data).

61 The trimeric spike glycoprotein (S) of SARS-CoV-2 binds its cellular receptor, angiotensin  
62 converting enzyme 2 (ACE2), through a receptor-binding domain (RBD), which is part of its  
63 N-terminal furin cleavage fragment (S1)<sup>3,4</sup>. S rearranges to translocate the virus into cells by  
64 membrane fusion<sup>5,6</sup>. The C-terminal furin cleavage fragment (S2) contains the fusion  
65 machinery<sup>7</sup>. Membrane fusion can be blocked by mutating S residues 986 and 987 to prolines,  
66 producing an S antigen stabilised in the prefusion conformation (P2 S)<sup>8-10</sup>. The RBD is a key  
67 target for virus neutralising antibodies, with an 'up' conformation, in which more neutralising  
68 epitopes are exposed, and a 'down' conformation in which many epitopes are buried<sup>5,10-12</sup>. In  
69 addition, some neutralising antibodies bind S epitopes outside the RBD.

70 During this pandemic, fast vaccine availability is critical. COVID-19 vaccine candidates based  
71 on different platforms are already in clinical trials, with the most advanced based on viral vector  
72 and nucleic acid technologies<sup>13-16</sup>. We report the preclinical development of BNT162b2, a lipid-  
73 nanoparticle (LNP) formulated N<sup>1</sup>-methyl-pseudouridine (m<sup>1</sup> $\Psi$ ) nucleoside-modified mRNA  
74 (modRNA) vaccine candidate that encodes P2 S with a native furin cleavage site resulting in  
75 the S1 and S2 cleavage fragments (Fig. 1a). The m<sup>1</sup> $\Psi$ -modification dampens innate immune  
76 sensing, and, together with optimised non-coding sequence elements, increases RNA  
77 translation *in vivo*<sup>17-19</sup>. ModRNA vaccines have already proven immunogenic for several viral  
78 targets<sup>20,21</sup>. BNT162b2 has been evaluated in phase 1 clinical trials in the US (NCT04368728)  
79 and Germany (NCT04380701, EudraCT: 2020-001038-36), and is now being evaluated in a  
80 pivotal, global, phase 2/3 safety and efficacy study<sup>15</sup>.

## 81 **Results**

82 BNT162b2 RNA *in vitro* transcribed by T7 polymerase from a plasmid DNA template has a  
83 single, sharp-peak microfluidic capillary electrophoresis profile, consistent with its calculated  
84 length of 4,283 nucleotides, indicating purity and integrity (Fig. 1b). When HEK293T/17 cells  
85 were incubated with BNT162b2 (which is LNP-formulated) or with BNT162b2 RNA mixed  
86 with a transfection reagent, robust expression of P2 S was detectable by flow cytometry  
87 (Extended Data Fig. 1a).

88 For structural characterisation, P2 S was expressed in Expi293F cells from DNA that encodes  
89 the same amino acid sequence as BNT162b2 RNA, with the addition of a C-terminal TwinStrep  
90 tag for affinity purification. The trimeric P2 S bound the human ACE2 peptidase domain (PD),  
91 and an anti-RBD human neutralising antibody B38 with high affinity ( $K_D$  1 nM, Extended Data  
92 Fig. 1b,c)<sup>22</sup>. Structural analysis by cryo-electron microscopy (cryo-EM) produced a 3.29 Å  
93 nominal resolution mass density map, into which a previously published atomic model<sup>10</sup> was  
94 fitted and rebuilt (Fig. 1c,d; Extended Data Fig. 2, Extended Data Table 1). The rebuilt model  
95 shows good agreement with reported structures of prefusion full-length wild type S and its  
96 ectodomain with P2 mutations<sup>5,10</sup>. Three-dimensional classification of the dataset showed a  
97 class of particles that was in the one RBD ‘up’ (accessible for receptor binding), two RBD  
98 ‘down’ (closed) conformation and represented 20.4% of the trimeric molecules. The remainder  
99 were in the all RBD ‘down’ conformation (Fig. 1e, Extended Data Fig. 2c). The RBD in the  
100 ‘up’ conformation was less well resolved than other parts of the structure, suggesting  
101 conformational flexibility and a dynamic equilibrium between RBD ‘up’ and RBD ‘down’  
102 states as also suggested by others<sup>5,23</sup>. Nevertheless, the binding and structural analyses indicate  
103 that the BNT162b2 RNA sequence encodes a recombinant P2 S that authentically presents the  
104 ACE2 binding site and other epitopes targeted by SARS-CoV-2 neutralising antibodies.

105 To characterise BNT162b2-elicited B- and T-cell responses, BALB/c mice were immunized  
106 intramuscularly (IM) once with 0.2, 1, or 5 µg BNT162b2 or received a buffer control. S1- and  
107 RBD-binding serum IgG developed rapidly at all dose levels in a dose-dependent manner. For  
108 S1-binding antibodies, the geometric mean concentration (GMC) in the 5 µg group was 386  
109 µg/mL at Day 28 (Fig. 2a, Extended Data Fig. 3a). At Day 28 after immunisation, vaccine-  
110 elicited IgG had a strong binding affinity for S1 (geometric mean  $K_D$  12 nM) and the RBD  
111 (geometric mean  $K_D$  0.99 nM), with both having a low off-rate (Extended Data Fig. 3b). SARS-  
112 CoV-2 neutralising activity in mouse serum was measured by a vesicular stomatitis virus

113 (VSV)-based SARS-CoV-2 pseudovirus neutralisation assay. Fifty percent pseudovirus  
114 neutralisation geometric mean titers (pVNT<sub>50</sub> GMTs) increased steadily after immunisation to  
115 26, 176, and 296 on Day 28 for the 0.2, 1, and 5 µg dose levels, respectively (Fig. 2b, Extended  
116 Data Fig. 3c).

117 A high fraction of splenocytes of CD4<sup>+</sup> and CD8<sup>+</sup> T-cell phenotype isolated from mice on Days  
118 12 and 28 after BNT162b2-immunisation had a strong antigen-specific IFN $\gamma$  and IL-2 response  
119 in ELISpot and intracellular cytokine staining flow cytometry analysis when re-stimulated *ex*  
120 *vivo* with a full-length S peptide pool (Fig. 2c-e). Total splenocytes harvested on Day 28 and  
121 *ex vivo* re-stimulated with the full-length S peptide pool secreted high levels of the T<sub>H</sub>1  
122 cytokines IL-2 or IFN $\gamma$ , but minute amounts of the T<sub>H</sub>2 cytokines IL-4, IL-5 and IL-13 as  
123 measured in multiplex immunoassays (Fig. 2f).

124 BNT162b2-induced effects on proliferation and dynamics of immune cell populations were  
125 assessed in injection site draining lymph nodes (dLNs), which are the principal immune-  
126 educated compartments for proficient T- and B-cell priming, and in blood and spleen for  
127 evaluation of its systemic effects. Higher numbers of plasma cells, class switched IgG1- and  
128 IgG2a-positive B cells, and germinal center B cells were observed in dLNs and spleens of mice  
129 12 days after immunisation with 5 µg BNT162b2 than after immunisation with buffer  
130 (Extended Data Fig. 4a, b). In Day 7 post-immunisation blood, there were significantly fewer  
131 circulating B cells than in blood from buffer-immunised mice (Extended Data Fig. 4c), which  
132 may imply that B-cell homing to lymphoid compartments augments B cell counts in dLN and  
133 spleen. The dLNs from BNT162b2-immunised mice also have significantly elevated counts of  
134 CD8<sup>+</sup> and CD4<sup>+</sup> T cells, which was most pronounced for T follicular helper (T<sub>FH</sub>) cells,  
135 including ICOS<sup>+</sup> subsets essential for germinal center formation (Extended Data Fig. 4a)<sup>24</sup>.  
136 BNT162b2 immunisation increased CD8<sup>+</sup> T cell counts in the blood and T<sub>FH</sub> cell counts in the  
137 spleen and blood (Extended Data Fig. 4b, c). These data indicate that BNT162b2 concurrently  
138 elicits strong SARS-CoV-2 pseudovirus neutralising titers and systemic T<sub>H</sub>1-driven CD4<sup>+</sup> and  
139 CD8<sup>+</sup> T-cell responses.

140 To assess BNT162b2-mediated protection in non-human primates, groups of six male, 2-4 year  
141 old rhesus macaques were immunised IM with 30 or 100 µg of BNT162b2 or saline control on  
142 Days 0 and 21. S1-binding IgG was readily detectable by Day 21 after Dose 1, and levels  
143 increased further after Dose 2 through Day 28 (Fig. 3a). Seven days after Dose 2 (Day 28), the  
144 GMCs of S1-binding IgG were 30,339 units (U)/mL (30 µg dose level) and 34,668 U/mL

145 (100 µg dose level). For comparison, the S1-binding IgG GMC of a panel of 38 SARS-CoV-2  
146 convalescent human sera was 631 U/mL, substantially lower than the GMCs of the immunised  
147 rhesus macaques after one or two doses.

148 Fifty percent virus neutralisation GMTs, measured by an authentic SARS-CoV-2 neutralisation  
149 assay<sup>25</sup>, were detectable in rhesus macaque sera by Day 21 after Dose 1 and peaked at a GMT  
150 of 962 (Day 35, 14 days after Dose 2 of 30 µg) or 1,689 (Day 28, 7 days after Dose 2 of 100 µg;  
151 Fig. 3b). Robust GMTs of 285 for 30 µg and 310 for 100 µg dose levels persisted to at least  
152 Day 56 (most recent time point tested). For comparison, the neutralisation GMT of the human  
153 convalescent serum panel was 94.

154 S-specific T-cell responses were analysed in BNT162b2-immunised rhesus macaques and  
155 saline-immunised controls by ELISpot and intracellular cytokine staining (ICS). Peripheral  
156 blood mononuclear cells (PBMCs) were collected before immunisation and at the times  
157 indicated after Doses 1 and 2. Strong IFN $\gamma$  but minimal IL-4 responses were detected by  
158 ELISpot after Dose 2 (Fig. 3c,d, Extended Data Fig. 5). ICS confirmed that BNT162b2 elicited  
159 strong S-specific IFN $\gamma$  producing T-cell responses, including a high frequency of CD4<sup>+</sup> T cells  
160 that produced IFN $\gamma$ , IL-2, and TNF but a low frequency of CD4<sup>+</sup> T cells that produced IL-4,  
161 indicating a T<sub>H1</sub>-biased response (Fig. 3e,f). BNT162b2 also elicited S-specific  
162 IFN $\gamma$ <sup>+</sup> producing CD8<sup>+</sup> T cells (Fig. 3g).

163 Six rhesus macaques that had received two immunisations with 100 µg BNT162b2 and three  
164 age-matched macaques that had received saline were challenged 55 days after Dose 2 with  
165  $1.05 \times 10^6$  plaque forming units of SARS-CoV-2 (strain USA-WA1/2020), split equally  
166 between intranasal and intratracheal routes, as previously described<sup>26</sup>. Three additional non-  
167 immunised, age-matched rhesus macaques (sentinels) were mock-challenged with cell culture  
168 medium. Nasal and oropharyngeal (OP) swabs were collected and bronchoalveolar lavage  
169 (BAL) was performed at the times indicated, and samples were tested for SARS-CoV-2 RNA  
170 (genomic RNA or subgenomic transcripts) by reverse-transcription quantitative polymerase  
171 chain reaction (RT-qPCR; Fig. 4). All personnel performing clinical, radiological,  
172 histopathological, or RT-qPCR evaluations were blinded to the group assignments of the  
173 macaques.

174 Viral RNA was detected in BAL fluid from 2 of the 3 control-immunised macaques on Day 3  
175 after challenge and from 1 of 3 on Day 6 (Fig. 4a). At no time point sampled was viral RNA

176 detected in BAL fluid from the BNT162b2-immunised and SARS-CoV-2 challenged macaques  
177 (Fig. 4a). The difference in viral RNA detection in BAL fluid between BNT162b2-immunised  
178 and control-immunised rhesus macaques after challenge is highly statistically significant (by a  
179 nonparametric test,  $p=0.0014$ ).

180 From control-immunised macaques, viral RNA was detected in nasal swabs obtained on Days  
181 1, 3, and 6 after SARS-CoV-2 challenge; from BNT162b2-immunised macaques, viral RNA  
182 was detected only in nasal swabs obtained on Day 1 after challenge and not in swabs obtained  
183 on Day 3 or subsequently (Fig. 4b). The pattern of viral RNA detection from OP swabs was  
184 similar to that for nasal swabs (Fig. 4c).

185 In general, virus-challenged animals showed no clinical signs of significant disease. We  
186 conclude that the 2-4 year old male rhesus macaque challenge model is primarily a SARS-CoV-  
187 2 infection model and not a COVID-19 disease model.

## 188 **Discussion**

189 We demonstrate that BNT162b2, an LNP-formulated, m1 $\Psi$  nucleoside-modified mRNA  
190 encoding SARS-CoV-2 S captured in a prefusion conformation is highly immunogenic in mice  
191 and rhesus macaques. Expression from DNA of protein with the BNT162b2-encoded amino  
192 acid sequence confirmed the P2 S prefusion conformation by cryo-EM. This analysis confirmed  
193 that the antigenically important RBD can assume the ‘up’ conformation, with the receptor  
194 binding site, rich in neutralising epitopes, accessible in a proportion of the molecules<sup>27</sup>. The  
195 alternative states observed likely reflect a dynamic equilibrium between RBD ‘up’ and ‘down’  
196 positions<sup>10,23</sup>. Binding of expressed and purified P2 S to ACE2 and a neutralising monoclonal  
197 antibody further demonstrates its conformational and antigenic integrity.

198 In mice, a single injection of BNT162b2 elicited high neutralizing titers and strong T<sub>H</sub>1 and T<sub>FH</sub>  
199 type CD4<sup>+</sup> and IFN $\gamma$ <sup>+</sup>IL-2<sup>+</sup> CD8<sup>+</sup> T-cell responses. Both BNT162b2 induced CD4<sup>+</sup> T-cell types  
200 may support antigen-specific antibody generation and maturation, and potentially protection  
201 from infectious challenge. Limitation and clearance of virus infection is promoted by the  
202 interplay of neutralising antibodies with CD8<sup>+</sup> T cells that eliminate intracellular virus  
203 reservoirs. CD8<sup>+</sup> T cells may also reduce the influx of monocytes into infected lung tissue,  
204 which can be associated with undesirable IL-6 and TNF production and impaired antigen  
205 presentation<sup>28,29</sup>. The contributions of the immune effector systems to human protection from



206 SARS-CoV-2 is not yet understood. Therefore, it appears prudent to develop COVID-19  
207 vaccines that enlist concomitant cognate B cell, CD4<sup>+</sup> T cell, and CD8<sup>+</sup> T-cell responses.

208 The immunogenicity of BNT162b2 in rhesus macaques paralleled its immunogenicity in mice.  
209 Seven days after Dose 2 of 100 µg, the neutralising GMT reached 18-times that of a human  
210 SARS-CoV-2 convalescent serum panel and remained 3.3-times higher than this benchmark  
211 five weeks after the last immunisation. The strongly T<sub>H</sub>1-biased CD4<sup>+</sup> T-cell response and  
212 IFNγ<sup>+</sup> CD8<sup>+</sup> T-cell response to BNT162b2 is a pattern favoured for vaccine safety and efficacy,  
213 providing added reassurance for clinical translation<sup>30</sup>. BNT162b2 protected 2-4 year old rhesus  
214 macaques from infectious SARS-CoV-2 challenge, with reduced detection of viral RNA in  
215 immunised animals compared to those that received saline and with no evidence of clinical  
216 exacerbation. Strong RT-qPCR evidence for lower respiratory tract protection was  
217 demonstrated by the absence of detectable SARS-CoV-2 RNA in serial BAL samples obtained  
218 starting 3 days after challenge of BNT162b2-immunised rhesus macaques.

219 We recently presented data from immunisation with BNT162b1, a vaccine candidate that has  
220 the same LNP-formulated m1Ψ nucleoside-modified RNA platform but expresses a trimerised,  
221 secreted RBD (Vogel et al., manuscript in preparation). The pattern, magnitude and durability  
222 of humoral and cellular responses to BNT162b1 in mice and macaques were in the range of  
223 those elicited by BNT162b2, as was protection of macaques from virus challenge, indicating  
224 that these features are largely class-intrinsic for this particular vaccine platform. BNT162b1  
225 elicits high SARS-CoV-2 neutralizing titers and strong T<sub>H</sub>1-biased CD4<sup>+</sup> and IFNγ<sup>+</sup> and IL-2<sup>+</sup>  
226 CD8<sup>+</sup> T cell responses in humans, consistent with the preclinical findings<sup>15,31,32</sup>.

227 The selection of BNT162b2 over BNT162b1 for further clinical testing was largely driven by  
228 greater tolerability of BNT162b2 with comparable immunogenicity in clinical trials<sup>15</sup> and the  
229 broader range of T-cell epitopes on the much larger full length spike. A global, pivotal, phase  
230 3 safety and efficacy study of immunisation with BNT162b2 (NCT04368728) is now well  
231 under way and may answer those open questions that cannot be addressed by preclinical  
232 models.

233



## 234 **Materials and Methods**

### 235 **Ethics statement.**

236 All mouse studies were performed at BioNTech SE, and protocols were approved by the local  
237 authorities (local welfare committee), conducted according to FELASA recommendations and  
238 in compliance with the German Animal Welfare Act and Directive 2010/63/EU. Only animals  
239 with an unobjectionable health status were selected for testing procedures.

240 Immunisations for the non-human primate (NHP) study were performed at the University of  
241 Louisiana at Lafayette-New Iberia Research Center (NIRC), which is accredited by the  
242 Association for Assessment and Accreditation of Laboratory Animal Care (AAALAC, Animal  
243 Assurance #: 000452). The work was in accordance with USDA Animal Welfare Act and  
244 Regulations and the NIH Guidelines for Research Involving Recombinant DNA Molecules, and  
245 Biosafety in Microbiological and Biomedical Laboratories. All procedures performed on these  
246 animals were in accordance with regulations and established guidelines and were reviewed and  
247 approved by an Institutional Animal Care and Use Committee or through an ethical review  
248 process. Infectious SARS-CoV-2 challenge for the NHP study was performed at the Southwest  
249 National Primate Research Center. Animal husbandry followed standards recommended by  
250 AAALAC International and the NIH Guide for the Care and Use of Laboratory Animals. This  
251 study was approved by the Texas Biomedical Research Institute Animal Care and Use  
252 Committee.

### 253 **Protein and peptide reagents.**

254 Purified recombinant SARS-CoV-2 S1 subunit including a histidine tag and the RBD tagged  
255 with the Fc region of human IgG1 (both Sino Biological) were used in ELISA to detect SARS-  
256 CoV-2 S-specific IgG in mice. Purified recombinant SARS-CoV-2 S1 and RBD with a histidine  
257 tag (both Sino Biological) were used for surface plasmon resonance (SPR) spectroscopy. An  
258 overlapping 15-mer peptide pool of the S protein was used for ELISpot, cytokine profiling and  
259 intracellular cytokine staining. An irrelevant peptide control (SPSYVYHQF, derived from gp70  
260 AH-1<sup>33</sup>) or a CMV peptide pool was used as control for ELISpot assays. All peptides were  
261 obtained from JPT Peptide Technologies.

262 **Human convalescent sera.**

263 Human COVID-19 convalescent sera (n=38) were drawn from donors 18-83 years of age at  
264 least 14 days after PCR-confirmed diagnosis and at a time when the participants were  
265 asymptomatic. Serum donors had symptomatic infections (35/38), or had had been hospitalised  
266 (1/38). Sera were obtained from Sanguine Biosciences (Sherman Oaks, CA), the MT group  
267 (Van Nuys, CA) and Pfizer Occupational Health and Wellness (Pearl River, NY) and used  
268 across different studies as reference benchmark.

269 **Cell culture.**

270 Human embryonic kidney (HEK)293T/17 and Vero 76 cells (both ATCC) were cultured in  
271 Dulbecco's modified Eagle's medium (DMEM) with GlutaMAX™ (Gibco) supplemented with  
272 10% fetal bovine serum (FBS [Sigma-Aldrich]). Cell lines were tested for mycoplasma  
273 contamination after receipt, before expansion and cryopreservation. For studies including NHP  
274 samples, Vero 76 and Vero CCL81 (both ATCC) cells were cultured in DMEM (Gibco)  
275 containing 2% HyClone fetal bovine and 100 U/mL penicillium/streptomycin (Gibco).  
276 Expi293F™ cells were grown in Expi293™ media and transiently transfected using  
277 ExpiFectamine™293 (all from Thermo Fisher Scientific).

278 ***In vitro* transcription and purification of RNA.**

279 To generate the template for RNA synthesis, a DNA fragment encoding the SARS-CoV-2 P2  
280 S protein (based on GenBank: MN908947), including the amino acid exchanges K986P and  
281 V987P, was cloned into a starting plasmid vector with backbone sequence elements for  
282 improved RNA stability and translational efficiency<sup>19,34</sup>. Non-coding backbone elements  
283 included the regions from the T7 promoter to the 5' and 3' UTR plus a poly(A) tail  
284 (100 nucleotides) interrupted by a linker (A30LA70, 10 nucleotides). The DNA was purified,  
285 spectrophotometrically quantified, and *in vitro* transcribed by T7 RNA polymerase in the  
286 presence of a trinucleotide cap1 analogue ((m<sub>2</sub><sup>7,3'-O</sup>)Gppp(m<sup>2'-O</sup>)ApG; TriLink) and of N<sup>1</sup>-  
287 methylpseudouridine-5'-triphosphate (m<sup>1</sup>ΨTP; Thermo Fisher Scientific) instead of uridine-  
288 5'-triphosphate (UTP)<sup>35</sup>. RNA was purified using magnetic particles<sup>36</sup>, integrity assessed by  
289 microfluidic capillary electrophoresis (Agilent Fragment Analyser), and concentration, pH,  
290 osmolality, endotoxin level and bioburden determined.

291 **Lipid-nanoparticle formulation of the RNA.**

292 Purified RNA was formulated into LNPs using an ethanolic lipid mixture of ionisable cationic  
293 lipid and transferred into an aqueous buffer system via diafiltration to yield an LNP composition  
294 similar to one previously described<sup>37</sup>. BNT162b2 was stored at -70 °C at a concentration of  
295 0.5 mg/mL.

296 **mRNA transfection and P2 S translation.**

297 HEK293T/17 cells were transfected with 1 µg RiboJuice transfection reagent-mixed  
298 BNT162b2 RNA or with BNT162b2 (BNT162b2 RNA formulated as LNP) by incubation for  
299 18 hours. Non-LNP formulated mRNA was diluted in Opti-MEM medium (Thermo Fisher  
300 Scientific) and mixed with the transfection reagents according to the manufacturer's  
301 instructions (RiboJuice, Merck Millipore). Transfected HEK293T/17 cells were stained with  
302 Fixable Viability Dye (eBioscience). After fixation (Fixation Buffer, BioLegend), cells were  
303 permeabilised (Perm Buffer, eBioscience) and stained with a monoclonal SARS-CoV-2 spike  
304 S1 antibody (SinoBiological). Cells were acquired on a FACSCanto II flow cytometer (BD  
305 Biosciences) using BD FACSDiva software version 8.0.1 and analysed by FlowJo software  
306 version 10.6.2 (FlowJo LLC, BD Biosciences).

307 **P2 S expression and purification.**

308 To express P2 S for structural characterisation, a gene encoding the full length of SARS-CoV-  
309 2 (GenBank: MN908947) with two prolines substituted at residues 986 and 987 followed with  
310 a C-terminal HRV3C protease site and a TwinStrep tag was cloned into a modified  
311 pcDNA3.1(+) vector with the CAG promoter. The TwinStrep-tagged P2 S was expressed in  
312 Expi293 cells. Purification of the recombinant protein was based on a procedure described  
313 previously, with minor modifications<sup>5</sup>. Upon cell lysis, P2 S was solubilized in 1% NP-40  
314 detergent. The TwinStrep-tagged protein was then captured with StrepTactin Sepharose HP  
315 resin in 0.5% NP-40. P2 S was further purified by size-exclusion chromatography and eluted  
316 as three distinct peaks in 0.02 % NP-40 as previously reported<sup>5</sup>. Peak 1, which consists of intact  
317 P2 S migrating at around 150 kDa, as well as dissociated S1 and S2 subunits, which co-migrate  
318 at just above 75 kDa, was used in the structural characterisation. Spontaneous dissociation of  
319 the S1 and S2 subunits mostly occurs throughout the course of the protein purification, starting  
320 at the point of detergent-mediated protein extraction.

321 **Biolayer interferometry.**

322 The binding of detergent NP-40 solubilized, purified P2 S to human ACE2 peptidase domain  
323 (ACE2 PD) and human neutralising monoclonal antibody B38<sup>22</sup> was performed on Octet  
324 RED384 (FortéBio) at 25 °C in a running buffer (RB) consisting of 25 mM Tris pH7.5, 150 mM  
325 NaCl, 1 mM EDTA and 0.02% NP-40. Avi-tagged ACE2-PD was captured on streptavidin  
326 coated sensors and B38 antibody was captured on sensors coated with protein G. After initial  
327 baseline equilibration of 120 s, the sensors were dipped in 10 µg/mL solution of Avi-tagged  
328 ACE2-PD or B38 mAb for 300 s to achieve capture levels of 1 nM using the threshold function.  
329 The sensors were dipped in RB for 120 s for collecting baseline before they were dipped in a  
330 concentration series of purified P2 S samples for 300 s (association phase). The sensors were  
331 immersed in RB for measuring 600 s (dissociation phase). Data were reference subtracted and  
332 fit to a 1:1 binding model with R<sup>2</sup> value greater than 0.95, to determine kinetics and affinity of  
333 binding, using Octet Data Analysis Software v10.0 (FortéBio).

#### 334 **Cryo-electron microscopy sample preparation, data collection and data processing.**

335 For TwinStrep-tagged P2 S, 4 µL purified protein at 0.5 mg/mL were applied to gold Quantifoil  
336 R1.2/1.3 300 mesh grids freshly overlaid with graphene oxide. Sample was blotted using a  
337 Vitrobot Mark IV for 4 s with a force of -2 before being plunged into liquid ethane cooled by  
338 liquid nitrogen. 27,701 micrographs were collected from a two identically prepared grids on a  
339 Titan Krios operating at 300 keV equipped with a Gatan K2 Summit direct electron detector in  
340 super-resolution mode at a magnification of 165,000x, for a magnified pixel size of 0.435 Å at  
341 the specimen level. Data were collected from each grid over a defocus range of -1.2 to -3.4 µm  
342 with a total electron dose of 50.32 and 50.12 e<sup>-</sup>/Å<sup>2</sup>, respectively, fractionated into 40 frames  
343 over a 6-second exposure for 1.26 and 1.25 e<sup>-</sup>/Å<sup>2</sup>/frame. On-the-fly motion correction, CTF  
344 estimation, and particle picking and extraction with a box size of 450 pixels were performed in  
345 Warp<sup>38</sup>, during which super-resolution data were binned to give a pixel size of 0.87 Å. A total  
346 of 1,119,906 particles were extracted. All subsequent processing was performed in RELION  
347 3.1-beta<sup>39</sup>. Particle heterogeneity was filtered out with 2D and 3D classification to filter out bad  
348 particles, yielding a set of 73,393 particles, which refined to 3.6 Å with C3 symmetry. 3D  
349 classification of this dataset without particle alignment separated out one class with a single  
350 RBD up, representing 15,098 particles. The remaining 58,295 particles, in three RBD ‘down’  
351 conformation, were refined to give a final model at 3.29 Å. The atomic model from PDB ID  
352 6XR8<sup>5</sup> was rigid-body fitted into the map density, then flexibly fitted to the density using real-  
353 space refinement in Phenix<sup>40</sup> alternating with manual building in Coot<sup>41</sup>. The cryo-EM model

354 validation is provided in Extended Data Fig 3b, the full cryo-EM data processing workflow in  
355 Extended Data Fig. 3c, and the model refinement statistics in Extended Data Table 1.

### 356 **Immunisation.**

357 *Mice.* Female BALB/c mice (Janvier; 8-12 weeks) and were randomly allocated to groups.  
358 BNT162b2 was diluted in PBS, 300 mM sucrose or saline (0.9% NaCl) and injected IM into  
359 the gastrocnemius muscle at a volume of 20  $\mu$ L under isoflurane anaesthesia.

360 *Rhesus macaques (Macaca mulatta).* Male rhesus macaques (2–4 years) were randomly  
361 assigned to receive either BNT162b2 or saline placebo control in 0.5 mL volume administered  
362 by IM injection in the left quadriceps muscle on Days 0 and 21.

### 363 **Tissue preparation.**

364 *Mice.* Peripheral blood was collected from the retro-orbital venous plexus under isoflurane  
365 anaesthesia or *vena facialis* without prior anaesthetisation. Blood was centrifuged for 5 minutes  
366 at 16,000 x g, and the serum was immediately used for downstream assays or stored at -20 °C.  
367 Spleen single-cell suspensions were prepared in PBS by mashing tissue against the surface of  
368 a 70  $\mu$ m cell strainer (BD Falcon). Erythrocytes were removed by hypotonic lysis. Popliteal,  
369 inguinal and iliac lymph nodes were pooled, cut into pieces, digested with collagenase D  
370 (1 mg/mL; Roche) and passed through cell strainers.

371 *Rhesus macaques (Macaca mulatta).* Serum was obtained before immunisation and on Days  
372 14, 21, 28, 35, 42, and 56. PBMCs were obtained before immunisation and on Days 7, 28, and  
373 42, except that PBMCs were not obtained from the buffer-immunised group on Day 28. Blood  
374 for serum and PBMCs was collected in compliance with animal protocol 2017-8725-023  
375 approved by the NIRC Institutional Animal Care and Use Committee. Animals were  
376 anaesthetised with ketamine HCl (10 mg/kg; IM) during blood collection and immunisation, and  
377 monitored for adequate sedation.

### 378 **S1- and RBD-binding IgG assay.**

379 For mouse sera, MaxiSorp plates (Thermo Fisher Scientific) were coated with recombinant S1  
380 or RBD (100 ng/100  $\mu$ L) in sodium carbonate buffer, and bound IgG was detected using an  
381 HRP-conjugated secondary antibody and TMB substrate (Biotrend). Data collection was  
382 performed using a BioTek Epoch reader and Gen5 software version 3.0.9. For concentration  
383 analysis, the signal of the specific samples was correlated to a standard curve of an isotype

384 control. For rhesus macaque and human sera, a recombinant SARS-CoV-2 S1 containing a C-  
385 terminal Avitag™ (Acro Biosystems) was bound to streptavidin-coated Luminex microspheres.  
386 Bound rhesus macaque or human anti-S1 antibodies present in the serum were detected with a  
387 fluorescently labelled goat anti-human polyclonal secondary antibody (Jackson  
388 ImmunoResearch). Data were captured as median fluorescent intensities (MFIs) using a  
389 Bioplex200 system (Bio-Rad) and converted to U/mL antibody concentrations using a reference  
390 standard consisting of 5 pooled human COVID-19 convalescent serum samples (obtained >14  
391 days PCR diagnosis), diluted in antibody depleted human serum with arbitrary assigned  
392 concentrations of 100 U/mL and accounting for the serum dilution factor.

### 393 **Binding kinetics of antigen-specific IgGs using surface plasmon resonance spectroscopy**

394 Binding kinetics of murine S1- and RBD-specific serum IgGs was determined using a Biacore  
395 T200 device (Cytiva) with HBS-EP running buffer (BR100669, Cytiva) at 25 °C. Carboxyl  
396 groups on the CM5 sensor chip matrix were activated with a mixture of 1-ethyl-3-(3-  
397 dimethylaminopropyl) carbodiimidehydrochloride (EDC) and N-hydroxysuccinimide (NHS) to  
398 form active esters for the reaction with amine groups. Anti-mouse-Fc-antibody (Jackson  
399 ImmunoResearch) was diluted in 10 mM sodium acetate buffer pH 5 (30 µg/mL) for covalent  
400 coupling to immobilisation level of ~10,000 response units (RU). Free N-hydroxysuccinimide  
401 esters on the sensor surface were deactivated with ethanolamine.

402 Mouse serum was diluted 1:50 in HBS-EP buffer and applied at 10 µL/min for 30 seconds to  
403 the active flow cell for capture by immobilised antibody, while the reference flow cell was  
404 treated with buffer. Binding analysis of captured murine IgG antibodies to S1-His or RBD-His  
405 (Sino Biological) was performed using a multi-cycle kinetic method with concentrations  
406 ranging from 25 to 400 nM or 1.5625 to 50 nM, respectively. An association period of 180  
407 seconds was followed by a dissociation period of 600 seconds with a constant flow rate of 40  
408 µL/min and a final regeneration step. Binding kinetics were calculated using a global kinetic fit  
409 model (1:1 Langmuir, Biacore T200 Evaluation Software Version 3.1, Cytiva).

### 410 **VSV-SARS-CoV-2 spike variant pseudovirus neutralisation.**

411 A recombinant replication-deficient vesicular stomatitis virus (VSV) vector that encodes GFP  
412 instead of VSV-G (VSVΔG-GFP) was pseudotyped with SARS-CoV-2 S protein according to  
413 published pseudotyping protocols<sup>42,43</sup>. In brief, HEK293T/17 monolayers transfected to express  
414 SARS-CoV-2 S truncated of the C-terminal cytoplasmic 19 amino acids (SARS-CoV-2-S-



415 CA19) were inoculated with VSV $\Delta$ G-GFP vector. After incubation for 1 hour at 37 °C, the  
416 inoculum was removed and cells were washed with PBS before medium supplemented with  
417 anti-VSV-G antibody (clone 8G5F11, Kerafast Inc.) was added to neutralise residual input  
418 virus. VSV/SARS-CoV-2 pseudovirus-containing medium was harvested 20 hours after  
419 inoculation, 0.2  $\mu$ m filtered and stored at -80 °C.

420 Serial dilutions of mouse serum samples were prepared and pre-incubated for 10 minutes at  
421 room temperature with VSV/SARS-CoV-2 pseudovirus suspension ( $4.8 \times 10^3$  infectious units  
422 [IU]/mL) before transferring the mix to Vero 76 cells. Inoculated Vero-76 cells were incubated  
423 for 20 hours at 37 °C. Plates were placed in an IncuCyte Live Cell Analysis system (Sartorius)  
424 and incubated for 30 minutes prior to the analysis (IncuCyte 2019B Rev2 software). Whole  
425 well scanning for brightfield and GFP fluorescence was performed using a 4 $\times$  objective. The  
426 50% pseudovirus neutralisation titre (pVNT<sub>50</sub>) was reported as the reciprocal of the first serum  
427 dilution yielding a 50% reduction in GFP-positive infected cell number per well compared to  
428 the mean of the no serum pseudovirus positive control. Each serum sample dilution was tested  
429 in duplicates.

#### 430 **IFN $\gamma$ and IL-4 ELISpot.**

431 Murine ELISpot assays were performed with mouse IFN $\gamma$  ELISpot<sup>PLUS</sup> kits according to the  
432 manufacturer's instructions (Mabtech). A total of  $5 \times 10^5$  splenocytes was *ex vivo* restimulated  
433 with the full-length S peptide mix (0.1  $\mu$ g/mL final concentration per peptide) or controls  
434 (gp70-AH1 [SPSYVYHQF]<sup>33</sup>, 4  $\mu$ g/mL; Concanavalin A [ConA], 2  $\mu$ g/mL [Sigma]).  
435 Streptavidin-alkaline phosphatase (ALP) and BCIP/NBT-plus substrate were added, and spots  
436 counted using an ELISpot plate reader (ImmunoSpot® S6 Core Analyzer [CTL]). Spot numbers  
437 were evaluated using ImmunoCapture Image Acquisition Software V7.0 and ImmunoSpot  
438 7.0.17.0 Professional. Spot counts denoted too numerous to count by the software were set to  
439 1,500. For T-cell subtyping, CD8<sup>+</sup> T cells and CD4<sup>+</sup> T cells were isolated from splenocyte  
440 suspensions using MACS MicroBeads (CD8a [Ly-2] and CD4 [L3T4] [Miltenyi Biotec])  
441 according to the manufacturer's instructions.  $1 \times 10^5$  CD8<sup>+</sup> or CD4<sup>+</sup> T cells were subsequently  
442 restimulated with  $5 \times 10^4$  syngeneic bone marrow-derived dendritic cells loaded with full-  
443 length S peptide mix (0.1  $\mu$ g/mL final concentration per peptide) or cell culture medium as  
444 control. Purity of isolated T-cell subsets was determined by flow cytometry.

445 Rhesus macaque PBMCs were tested with commercially available NHP IFN $\gamma$  and IL-4 ELISpot  
446 assay kits (Mabtech, Sweden). Cryopreserved rhesus macaque PBMCs were thawed in pre-



447 warmed AIM-V media (Thermo Fisher Scientific, US) with Benzonase (EMD Millipore, US).  
448 For IFN $\gamma$  ELISpot,  $1.0 \times 10^5$  PBMCs and  $2.5 \times 10^5$  PBMCs for IL-4 ELISpot were stimulated  
449 *ex vivo* with 1  $\mu$ g/mL of the full-length S overlapping peptide mix. Tests were performed in  
450 triplicate wells and media-DMSO, a CMV peptide pool and PHA (Sigma) were included as  
451 controls. After 24 hours for IFN $\gamma$  and 48 hours for IL-4, Streptavidin-HRP and AEC substrate  
452 (BD Bioscience) were added, and spots counted using a CTL ImmunoSpot S6 Universal  
453 Analyzer (CTL, US). Results shown are background (Media-DMSO) subtracted and  
454 normalized to SFC/ $10^6$  PBMCs.

#### 455 **Flow cytometry for analysis of cell mediated immunity.**

456 For mouse T-cell analysis in peripheral blood, erythrocytes from 50  $\mu$ L freshly drawn blood  
457 were lysed (ACK lysing buffer [Gibco]), and cells were stained with Fixable Viability Dye  
458 (eBioscience) and primary antibodies in the presence of Fc block in flow buffer (DPBS [Gibco]  
459 supplemented with 2% FCS, 2 mM EDTA [both Sigma] and 0.01% sodium azide [Morphisto]).  
460 After staining with secondary biotin-coupled antibodies in flow buffer, cells were stained  
461 extracellularly against surface markers with directly labelled antibodies and streptavidin in  
462 Brilliant Stain Buffer Plus (BD Bioscience) diluted in flow buffer. Cells were washed with 2%  
463 RotiHistofix (Carl Roth), fixed (Fix/Perm Buffer, FoxP3/Transcription Factor Staining Buffer  
464 Set [eBioscience]) and permeabilised (Perm Buffer, FoxP3/Transcription Factor Staining  
465 Buffer Set [eBioscience]) overnight. Permeabilised cells were intracellularly treated with Fc  
466 block and stained with antibodies against transcription factors in Perm Buffer.

467 For mouse T-cell analysis in lymphoid tissues,  $1.5 \times 10^6$  lymph node and  $4 \times 10^6$  spleen cells  
468 were stained for viability and extracellular antigens with directly labelled antibodies. Fixation,  
469 permeabilisation and intracellular staining was performed as described for blood T-cell staining.

470 For mouse B-cell subtyping in lymphoid tissues,  $2.5 \times 10^5$  lymph node and  $1 \times 10^6$  spleen cells  
471 were treated with Fc block, stained for viability and extracellular antigens as described for blood  
472 T-cell staining and fixed with 2% RotiHistofix overnight.

473 For mouse intracellular cytokine staining in T cells,  $4 \times 10^6$  spleen cells were *ex vivo*  
474 restimulated with 0.5  $\mu$ g/mL final concentration per peptide of full-length S peptide mix or cell  
475 culture medium (no peptide) as control in the presence of GolgiStop and GolgiPlug (both BD  
476 Bioscience) for 5 hours. Cells were stained for viability and extracellular antigens as described

477 for lymphoid T-cell staining. Cells were fixed with 2% RotiHistofix and permeabilised  
478 overnight. Intracellular staining was performed as described for blood T-cell staining.

479 Mouse cells were acquired on a BD Symphony A3 or BD Celesta (B-cell subtyping) flow  
480 cytometer (BD Bioscience) using BD FACSDiva software version 9.1 or 8.0.1.1, respectively,  
481 and analysed with FlowJo 10.6 (FlowJo LLC, BD Biosciences).

482 For rhesus macaques intracellular cytokine staining in T cells,  $1.5 \times 10^6$  PBMCs were stimulated  
483 with the full-length S peptide mix at 1  $\mu\text{g}/\text{mL}$ , Staphylococcus enterotoxin B (SEB; 2  $\mu\text{g}/\text{mL}$ )  
484 as positive control, or 0.2% DMSO as negative control. GolgiStop and GolgiPlug (both BD  
485 Bioscience) were added. Following 37 °C incubation for 12 to 16 h, cells were stained for  
486 viability and extracellular antigens after blocking Fc binding sites with directly labelled  
487 antibodies. Cells were then fixed and permeabilized with BDCytoFix/CytoPerm solution (BD  
488 Bioscience), intracellular staining was performed in perm buffer for 30 min at RT. Cells were  
489 washed, resuspended in 2% FBS/PBS buffer and acquired on a LSR Fortessa. Data analyzed  
490 by FlowJo (10.4.1). Results shown are background (Media-DMSO) subtracted.

#### 491 **Cytokine profiling.**

492 Mouse splenocytes were re-stimulated for 48 hours with full-length S peptide mix (0.1  $\mu\text{g}/\text{mL}$   
493 final concentration per peptide) or cell culture medium (no peptide) as control. Concentrations  
494 of IFN $\gamma$ , IL-2, IL-4, IL-5 and IL-13 in supernatants were determined using a bead-based, 11-  
495 plex T<sub>H1</sub>/T<sub>H2</sub> mouse ProcartaPlex multiplex immunoassay (Thermo Fisher Scientific)  
496 according to the manufacturer's instructions. Fluorescence was measured with a Bioplex200  
497 system (Bio-Rad) and analysed with ProcartaPlex Analyst 1.0 software (Thermo Fisher  
498 Scientific). Values below the lower limit of quantification (LLOQ) were set to zero.

#### 499 **SARS-CoV-2 neutralisation.**

500 The SARS-CoV-2 neutralisation assay used a previously described strain of SARS-CoV-2  
501 (USA\_WA1/2020) that had been rescued by reverse genetics and engineered by the insertion  
502 of an mNeonGreen (mNG) gene into open reading frame 7 of the viral genome<sup>25</sup>. This reporter  
503 virus generates similar plaque morphologies and indistinguishable growth curves from wild-  
504 type virus. Viral master stocks were grown in Vero 76 cells as previously described<sup>44</sup>. When  
505 testing human convalescent serum specimens, the fluorescent neutralisation assay produced  
506 comparable results as the conventional plaque reduction neutralisation assay. Serial dilutions

507 of heat-inactivated sera were incubated with the reporter virus ( $2 \times 10^4$  PFU per well) to yield  
508 approximately a 10-30% infection rate of the Vero CCL81 monolayer for 1 hour at 37 °C before  
509 inoculating Vero CCL81 cell monolayers (targeted to have 8,000 to 15,000 cells in the central  
510 field of each well at the time of seeding, one day before infection) in 96-well plates to allow  
511 accurate quantification of infected cells. Cell counts were enumerated by nuclear stain (Hoechst  
512 33342) and fluorescent virally infected foci were detected 16-24 hours after inoculation with a  
513 Cytation 7 Cell Imaging Multi-Mode Reader (Biotek) with Gen5 Image Prime version 3.09.  
514 Titers were calculated in GraphPad Prism version 8.4.2 by generating a 4- parameter (4PL)  
515 logistical fit of the percent neutralisation at each serial serum dilution. The 50% neutralisation  
516 titre (VNT<sub>50</sub>) was reported as the interpolated reciprocal of the dilution yielding a 50%  
517 reduction in fluorescent viral foci.

#### 518 **SARS-CoV-2 challenge of rhesus macaques (*Macaca mulatta*).**

519 The SARS-CoV-2 inoculum was obtained from a stock of  $2.1 \times 10^6$  PFU/mL previously  
520 prepared at Texas Biomedical Research Institute (San Antonio, TX), aliquoted into single use  
521 vials, and stored at -70 °C. The working virus stock was generated from two passages of the  
522 SARS-CoV-2 USA-WA1/2020 isolate (a 4<sup>th</sup> passage seed stock purchased from BEI Resources;  
523 NR-52281) in Vero 76 cells. The virus was confirmed to be SARS-CoV-2 by deep sequencing  
524 and identical to the published sequence (GenBank accession number MN985325.1).  
525 BNT162b2-immunised (n=6) and age-matched saline control-immunised (n=3) male rhesus  
526 macaques (control) were challenged with  $1.05 \times 10^6$  plaque forming units of SARS-CoV-2  
527 USA-WA1/2020 isolate, split equally between the intranasal (IN; 0.25 mL) and intratracheal  
528 (IT; 0.25 mL) routes as previously described<sup>26</sup>. The challenge was performed 55 days after the  
529 second immunisation. A separate sentinel group of non-immunised age- and sex-matched  
530 animals (n=3) was mock challenged with DMEM supplemented with 10% FCS IN (0.25 mL)  
531 and IT (0.25 mL). Approximately two weeks prior to challenge, animals were moved to the  
532 ABSL-3 facility at Southwest National Primate Research Center (SNPRC; San Antonio, TX).  
533 Animals were monitored regularly by a board-certified veterinary clinician for rectal body  
534 temperature, weight and physical examination. Specimen collection was performed under  
535 tiletamine zolazepam (Telazol) anaesthesia as described<sup>26</sup>. Nasal and oropharyngeal swabs  
536 were collected from all macaques at Day 0, 1, 3, and 6 (relative to the day of challenge), from  
537 BNT162b2-immunised macaques on Day 7 or 8, and from control and sentinel macaques on

538 Day 10. Bronchoalveolar lavage (BAL) was performed on all macaques the week before  
539 challenge and on Days 3 and 6 post-challenge and on BNT162b2-immunised macaques on Day  
540 7 or 8. BAL was performed by instilling four times 20 mL of saline. These washings were  
541 pooled, aliquoted and stored frozen at -70 °C. Necropsy was performed on BNT162b2-  
542 immunised animals on Day 7 or 8. Control and sentinel animals were not necropsied to allow  
543 re-challenge (control) or challenge (sentinel) on a subsequent day.

#### 544 **Reverse-transcription quantitative polymerase chain reaction.**

545 To detect and quantify SARS-CoV-2 in NHP, viral RNA was extracted from nasal swabs, OP  
546 swabs, and BAL specimens as previously described<sup>45-47</sup> and tested by RT-qPCR as previously  
547 described<sup>26</sup>. Briefly, 10 µg yeast tRNA and  $1 \times 10^3$  PFU of MS2 phage (*Escherichia coli*  
548 bacteriophage MS2, ATCC) were added to each thawed sample, and RNA extraction performed  
549 using the NucleoMag Pathogen kit (Macherey-Nagel). The SARS-CoV-2 RT-qPCR was  
550 performed on extracted RNA using a CDC-developed 2019-nCoV\_N1 assay on a QuantStudio  
551 3 instrument (Applied Biosystems). The cut-off for positivity (limit of detection, LOD) was  
552 established at 10 gene equivalents (GE) per reaction (800 GE/mL). Samples were tested in  
553 duplicate. On day 6, one BAL specimen from the control group and one day 1 nasal swab from  
554 the BNT162b1-immunised group had, on repeated measurements, viral RNA levels on either  
555 side of the LLOD. These specimens were categorised as indeterminate and excluded from the  
556 graphs and the analysis.

#### 557 **Statistics and reproducibility.**

558 No statistical methods were used to predetermine group and samples sizes (n). All experiments  
559 were performed once. P-values reported for RT-qPCR analysis were determined by  
560 nonparametric analysis (Friedman's test) based on the ranking of viral RNA shedding data  
561 within each day. PROC RANK and PROC GLM from SAS® 9.4 were used to calculate the p-  
562 values. Samples from post challenge days (Days 3, 6 and end of protocol [EOP] for BAL; Days  
563 1, 3, 6 and 10 [control and sentinel] or EOP [BNT162b2-immunised] for nasal and  
564 oropharyngeal swabs) were included in the analysis. Indeterminate results were excluded from  
565 this analysis. All remaining analyses were carried out using GraphPad Prism 8.4.

566 **Data availability.**

567 The data that support the findings of this study are available from the corresponding author  
568 upon reasonable request.

569 **Acknowledgements**

570 We thank T. Garretson for advice on NHP serology studies, R. F. Sommese and K. F. Fennell  
571 for technical assistance for molecular cloning and cell based binding. Valuable support and  
572 assistance from R. de la Caridad Güimil Garcia<sup>1</sup>, A. Su, M. Dvorak, M. Drude, F. Zehner, T.  
573 Lapin, B. Ludloff, S. Hinz, F. Bayer, J. Scholz, A.L. Ernst, T. Sticker and S. Wittig resulted in  
574 a rapid availability of oligonucleotides and DNA templates. E. Boehm, K. Goebel, R. Frieling,  
575 C. Berger, S. Koch, T. Wachtel, J. Leilich, M. Mechler, R. Wysocki, M. Le Gall, A. Czech and  
576 S. Klenk carried out RNA production and analysis. Without their commitment during this  
577 pandemic situation, this vaccine candidate could not have been transferred to non-clinical  
578 studies in light speed. B. Weber, J. Vogt, S. Krapp, K. Zwadlo, J. Mottl, J. Mühl and P.  
579 Windecker supported the mouse studies and serological analysis with excellent technical  
580 assistance. We thank A. Ota-Setlik for ELISpot testing of NHP samples. Radiologists A. K.  
581 Voges, M. R. Gutman and E. Clemmons advised on the radiographic scoring. We thank  
582 Polymun Scientific for excellent formulation services as well as Acuitas Therapeutics for  
583 fruitful discussions.

584 **Author Contributions**

585 U.S. conceived and conceptualised the work and strategy. S.He., S.C.D., C.K. and M.C.G.  
586 designed primers and cloned all constructs. T.Z., S.F., J.S. and A.N.K. developed, planned,  
587 performed and supervised RNA synthesis and analysis. E.H.M. purified P2 S. P.V.S. developed  
588 and performed biolayer interferometry. J.A.L. and S.H. performed electron microscopy and  
589 solved the structure of the complex. Y.C. supervised the structural and biophysical  
590 characterisation and analysed the structures. A.M. and B.G.L. performed surface plasmon  
591 resonance spectroscopy. A.G. and S.A.K. planned, performed and analysed *in vitro* studies.  
592 F.B., T.K., C.R. managed formulation strategy. A.B.V., M.V., L.M.K. designed mouse studies  
593 and analysed and interpreted data. A.P., S.E., D.P. and G.S. performed and analysed the S1-  
594 binding IgG assays. R.C., Jr. and K.J.A. performed and analysed viral RT-qPCR data. A.M.,

595 B.S., A.W., C.F.-G. and P.-Y.S. performed and analysed pVNT and VNT assays. D.E., D.S.,  
596 B.J., Y.F., H.J. performed *in vivo* studies and ELISpot assays. A.B.V., K.C.W., J.L., M.S.M. and  
597 M.V. planned, analysed and interpreted ELISpot assays. L.M.K., J.L., D.E., Y.F., H.J., A.P.H.  
598 M.S.M. and P.A. planned, performed and analysed flow cytometry assays. A.B.V., L.M.K., Y.F.  
599 and H.J. planned, performed, analysed and interpreted cytokine release assays. I.K., K.A.S.,  
600 K.T., D.K. and P.R.D. designed NHP studies and analysed and interpreted data. K.T., M.P.,  
601 I.L.S. and W.K. oversaw NHP immunogenicity and serology testing. S.H.-U. and K.B. provided  
602 veterinary services for NHPs. J.C., T.C. and J.O. managed the NHP colony. A.B.V., I.K., Y.C.,  
603 A.M., M.V., L.M.K., C.T., K.S., Ö.T., P.R.D., K.U.J. and U.S. wrote the manuscript. All authors  
604 supported the review of the manuscript.

## 605 **Competing interests**

606 The authors declare: U.S. and Ö.T. are management board members and employees at  
607 BioNTech SE (Mainz, Germany); K.C.W., B.G.L., D.S., B.J., T.K. and C.R. are employees at  
608 BioNTech SE; A.B.V., A.M., M.V., L.M.K., S.He., A.G., T.Z., A.P., D.E., S.C.D., S.F., S.E.,  
609 F.B., B.S., A.W., Y.F., H.J., S.A.K., A.P.H., P.A., J.S., C.K., and A.N.K. are employees at  
610 BioNTech RNA Pharmaceuticals GmbH (Mainz, Germany); A.B.V., A.M., K.C.W., A.G., S.F.,  
611 A.N.K. and U.S. are inventors on patents and patent applications related to RNA technology and  
612 COVID-19 vaccine; A.B.V., A.M., M.V., L.M.K., K.C.W., S.He., B.G.L., A.P., D.E., S.C.D.,  
613 S.F., S.E., D.S., B.J., B.S., A.P.H., P.A., J.S., C.K., T.K., C.R., A.N.K., Ö.T. and U.S. have  
614 securities from BioNTech SE; I.K., Y.C., K.A.S., J.L., M.M., K.T., M.C.G., S.H.,  
615 J.A.L., E.H.M., P.V.S., C.Y.T., D.P., G.S., M.P., I.L.S., T.C., J.O., W.V.K., P.R.D. and K.U.J.  
616 are employees of Pfizer and may hold stock options;

617 C.F.-G. and P.-Y.S. received compensation from Pfizer to perform neutralisation assays;

618 J.C., S.H.-U., K.B., R.C., jr., K.J.A. and D.K., are employees of Southwest National Primate  
619 Research Center, which received compensation from Pfizer to conduct the animal challenge  
620 work;

621 no other relationships or activities that could appear to have influenced the submitted work.

622 **Funding**

623 BioNTech is the Sponsor of the study, and Pfizer it its agent. BioNTech and Pfizer are  
624 responsible for the design, data collection, data analysis, data interpretation, and writing of the  
625 report. The corresponding authors had full access to all the data in the study and had final  
626 responsibility for the decision to submit the data for publication. This study was not supported  
627 by any external funding at the time of submission.

628 **Additional Information**

629 Supplementary Information is available for this study.

630 Correspondence and requests for materials should be addressed to Ugur Sahin.

631

632



## 633 **References**

- 634 1. Zhu, N. *et al.* A Novel Coronavirus from Patients with Pneumonia in China, 2019. *The New*  
635 *England journal of medicine* **382**, 727–733; 10.1056/NEJMoa2001017 (2020).
- 636 2. Zhou, P. *et al.* A pneumonia outbreak associated with a new coronavirus of probable bat  
637 origin. *Nature* **579**, 270–273; 10.1038/s41586-020-2012-7 (2020).
- 638 3. Yan, R. *et al.* Structural basis for the recognition of SARS-CoV-2 by full-length human  
639 ACE2. *Science (New York, N.Y.)* **367**, 1444–1448; 10.1126/science.abb2762 (2020).
- 640 4. Yi, C. *et al.* Key residues of the receptor binding motif in the spike protein of SARS-CoV-  
641 2 that interact with ACE2 and neutralizing antibodies. *Cellular & molecular immunology*;  
642 10.1038/s41423-020-0458-z (2020).
- 643 5. Cai, Y. *et al.* Distinct conformational states of SARS-CoV-2 spike protein. *Science (New*  
644 *York, N.Y.)*; 10.1126/science.abd4251 (2020).
- 645 6. Ou, X. *et al.* Characterization of spike glycoprotein of SARS-CoV-2 on virus entry and its  
646 immune cross-reactivity with SARS-CoV. *Nature communications* **11**, 1620;  
647 10.1038/s41467-020-15562-9 (2020).
- 648 7. Fan, X., Cao, D., Kong, L. & Zhang, X. Cryo-EM analysis of the post-fusion structure of  
649 the SARS-CoV spike glycoprotein. *Nature communications* **11**, 3618; 10.1038/s41467-020-  
650 17371-6 (2020).
- 651 8. Kirchdoerfer, R. N. *et al.* Stabilized coronavirus spikes are resistant to conformational  
652 changes induced by receptor recognition or proteolysis. *Scientific reports* **8**, 15701;  
653 10.1038/s41598-018-34171-7 (2018).
- 654 9. Pallesen, J. *et al.* Immunogenicity and structures of a rationally designed prefusion MERS-  
655 CoV spike antigen. *Proceedings of the National Academy of Sciences of the United States*  
656 *of America* **114**, E7348-E7357; 10.1073/pnas.1707304114 (2017).
- 657 10. Wrapp, D. *et al.* Cryo-EM structure of the 2019-nCoV spike in the prefusion conformation.  
658 *Science (New York, N.Y.)* **367**, 1260–1263; 10.1126/science.abb2507 (2020).

- 659 11. Brouwer, P. J. M. *et al.* Potent neutralizing antibodies from COVID-19 patients define  
660 multiple targets of vulnerability. *Science (New York, N.Y.)*; 10.1126/science.abc5902  
661 (2020).
- 662 12. Chi, X. *et al.* A neutralizing human antibody binds to the N-terminal domain of the Spike  
663 protein of SARS-CoV-2. *Science (New York, N.Y.)*; 10.1126/science.abc6952 (2020).
- 664 13. Jackson, L. A. *et al.* An mRNA Vaccine against SARS-CoV-2 - Preliminary Report. *The*  
665 *New England journal of medicine*; 10.1056/NEJMoa2022483 (2020).
- 666 14. Zhu, F.-C. *et al.* Safety, tolerability, and immunogenicity of a recombinant adenovirus type-  
667 5 vectored COVID-19 vaccine. A dose-escalation, open-label, non-randomised, first-in-  
668 human trial. *The Lancet* **395**, 1845–1854; 10.1016/S0140-6736(20)31208-3 (2020).
- 669 15. Walsh, E. E. *et al.* RNA-Based COVID-19 Vaccine BNT162b2 Selected for a Pivotal  
670 Efficacy Study. *medRxiv 2020*; 10.1101/2020.08.17.20176651 (2020).
- 671 16. Folegatti, P. M. *et al.* Safety and immunogenicity of the ChAdOx1 nCoV-19 vaccine against  
672 SARS-CoV-2. A preliminary report of a phase 1/2, single-blind, randomised controlled trial.  
673 *The Lancet* **396**, 467–478; 10.1016/S0140-6736(20)31604-4 (2020).
- 674 17. Pardi, N. *et al.* Expression kinetics of nucleoside-modified mRNA delivered in lipid  
675 nanoparticles to mice by various routes. *Journal of controlled release : official journal of*  
676 *the Controlled Release Society* **217**, 345–351; 10.1016/j.jconrel.2015.08.007 (2015).
- 677 18. Karikó, K. *et al.* Incorporation of pseudouridine into mRNA yields superior  
678 nonimmunogenic vector with increased translational capacity and biological stability.  
679 *Molecular therapy : the journal of the American Society of Gene Therapy* **16**, 1833–1840;  
680 10.1038/mt.2008.200 (2008).
- 681 19. Orlandini von Niessen, A. G. *et al.* Improving mRNA-Based Therapeutic Gene Delivery by  
682 Expression-Augmenting 3' UTRs Identified by Cellular Library Screening. *Mol Ther* **27**,  
683 824–836; 10.1016/j.ymthe.2018.12.011 (2019).
- 684 20. Pardi, N. *et al.* Zika virus protection by a single low-dose nucleoside-modified mRNA  
685 vaccination. *Nature* **543**, 248–251; 10.1038/nature21428 (2017).

- 686 21. Pardi, N. *et al.* Characterization of HIV-1 Nucleoside-Modified mRNA Vaccines in Rabbits  
687 and Rhesus Macaques. *Molecular therapy. Nucleic acids* **15**, 36–47;  
688 10.1016/j.omtn.2019.03.003 (2019).
- 689 22. Wu, Y. *et al.* A noncompeting pair of human neutralizing antibodies block COVID-19 virus  
690 binding to its receptor ACE2. *Science (New York, N.Y.)* **368**, 1274–1278;  
691 10.1126/science.abc2241 (2020).
- 692 23. Henderson, R. *et al.* Controlling the SARS-CoV-2 spike glycoprotein conformation. *Nature*  
693 *structural & molecular biology*; 10.1038/s41594-020-0479-4 (2020).
- 694 24. Hutloff, A. Regulation of T follicular helper cells by ICOS. *Oncotarget* **6**, 21785–21786;  
695 10.18632/oncotarget.4798 (2015).
- 696 25. Muruato, A. E. *et al.* A high-throughput neutralizing antibody assay for COVID-19  
697 diagnosis and vaccine evaluation. *Nature communications* **11**, 4059; 10.1038/s41467-020-  
698 17892-0 (2020).
- 699 26. Singh, D. K. *et al.* SARS-CoV-2 infection leads to acute infection with dynamic cellular  
700 and inflammatory flux in the lung that varies across nonhuman primate species. *bioRxiv*  
701 *2020.06.05.136481*; 10.1101/2020.06.05.136481 (2020).
- 702 27. Zost, S. J. *et al.* Rapid isolation and profiling of a diverse panel of human monoclonal  
703 antibodies targeting the SARS-CoV-2 spike protein. *Nature medicine*; 10.1038/s41591-  
704 020-0998-x (2020).
- 705 28. Yang, D. *et al.* Attenuated interferon and pro-inflammatory response in SARS-CoV-2-  
706 infected human dendritic cells is associated with viral antagonism of STAT1  
707 phosphorylation. *The Journal of infectious diseases*; 10.1093/infdis/jiaa356 (2020).
- 708 29. Jafarzadeh, A., Chauhan, P., Saha, B., Jafarzadeh, S. & Nemati, M. Contribution of  
709 monocytes and macrophages to the local tissue inflammation and cytokine storm in COVID-  
710 19: Lessons from SARS and MERS, and potential therapeutic interventions. *Life sciences*,  
711 118102; 10.1016/j.lfs.2020.118102 (2020).

- 712 30. Lambert, P.-H. *et al.* Consensus summary report for CEPI/BC March 12-13, 2020 meeting:  
713 Assessment of risk of disease enhancement with COVID-19 vaccines. *Vaccine* **38**, 4783–  
714 4791; 10.1016/j.vaccine.2020.05.064 (2020).
- 715 31. Sahin, U. *et al.* Concurrent human antibody and T H 1 type T-cell responses elicited by a  
716 COVID-19 RNA vaccine. *medRxiv* 2020.07.17.20140533; 10.1101/2020.07.17.20140533  
717 (2020).
- 718 32. Mulligan, M. J. *et al.* Phase 1/2 study of COVID-19 RNA vaccine BNT162b1 in adults.  
719 *Nature*; 10.1038/s41586-020-2639-4 (2020).
- 720 33. Slansky, J. E. *et al.* Enhanced antigen-specific antitumor immunity with altered peptide  
721 ligands that stabilize the MHC-peptide-TCR complex. *Immunity* **13**, 529–538;  
722 10.1016/S1074-7613(00)00052-2 (2000).
- 723 34. Holtkamp, S. *et al.* Modification of antigen-encoding RNA increases stability, translational  
724 efficacy, and T-cell stimulatory capacity of dendritic cells. *Blood* **108**, 4009–4017;  
725 10.1182/blood-2006-04-015024 (2006).
- 726 35. Grudzien-Nogalska, E. *et al.* Synthetic mRNAs with superior translation and stability  
727 properties. *Methods in molecular biology (Clifton, N.J.)* **969**, 55–72; 10.1007/978-1-62703-  
728 260-5\_4 (2013).
- 729 36. Berensmeier, S. Magnetic particles for the separation and purification of nucleic acids.  
730 *Appl.Microbiol.Biotechnol.* **73**, 495–504; 10.1007/s00253-006-0675-0 (2006).
- 731 37. Maier, M. A. *et al.* Biodegradable lipids enabling rapidly eliminated lipid nanoparticles for  
732 systemic delivery of RNAi therapeutics. *Molecular therapy : the journal of the American*  
733 *Society of Gene Therapy* **21**, 1570–1578; 10.1038/mt.2013.124 (2013).
- 734 38. Tegunov, D. & Cramer, P. Real-time cryo-electron microscopy data preprocessing with  
735 Warp. *Nature methods* **16**, 1146–1152; 10.1038/s41592-019-0580-y (2019).
- 736 39. Zivanov, J. *et al.* New tools for automated high-resolution cryo-EM structure determination  
737 in RELION-3. *eLife* **7**; 10.7554/eLife.42166 (2018).

- 738 40. Adams, P. D. *et al.* PHENIX: a comprehensive Python-based system for macromolecular  
739 structure solution. *Acta crystallographica. Section D, Biological crystallography* **66**, 213–  
740 221; 10.1107/S0907444909052925 (2010).
- 741 41. Emsley, P., Lohkamp, B., Scott, W. G. & Cowtan, K. Features and development of Coot.  
742 *Acta crystallographica. Section D, Biological crystallography* **66**, 486–501;  
743 10.1107/S0907444910007493 (2010).
- 744 42. Lester, S. *et al.* Middle East respiratory coronavirus (MERS-CoV) spike (S) protein  
745 vesicular stomatitis virus pseudoparticle neutralization assays offer a reliable alternative to  
746 the conventional neutralization assay in human seroepidemiological studies. *Access*  
747 *Microbiology* **1**, 20290; 10.1099/acmi.0.000057 (2019).
- 748 43. Berger Rentsch, M. & Zimmer, G. A vesicular stomatitis virus replicon-based bioassay for  
749 the rapid and sensitive determination of multi-species type I interferon. *PLoS ONE* **6**,  
750 e25858; 10.1371/journal.pone.0025858 (2011).
- 751 44. Xie, X. *et al.* An Infectious cDNA Clone of SARS-CoV-2. *Cell host & microbe* **27**, 841-  
752 848.e3; 10.1016/j.chom.2020.04.004 (2020).
- 753 45. Gautam, U. S. *et al.* In vivo inhibition of tryptophan catabolism reorganizes the tuberculoma  
754 and augments immune-mediated control of Mycobacterium tuberculosis. *Proceedings of the*  
755 *National Academy of Sciences of the United States of America* **115**, E62-E71;  
756 10.1073/pnas.1711373114 (2018).
- 757 46. Mehra, S. *et al.* Granuloma correlates of protection against tuberculosis and mechanisms of  
758 immune modulation by Mycobacterium tuberculosis. *The Journal of infectious diseases*  
759 **207**, 1115–1127; 10.1093/infdis/jis778 (2013).
- 760 47. Joosten, S. A. *et al.* Mycobacterium tuberculosis peptides presented by HLA-E molecules  
761 are targets for human CD8 T-cells with cytotoxic as well as regulatory activity. *PLoS*  
762 *pathogens* **6**, e1000782; 10.1371/journal.ppat.1000782 (2010).

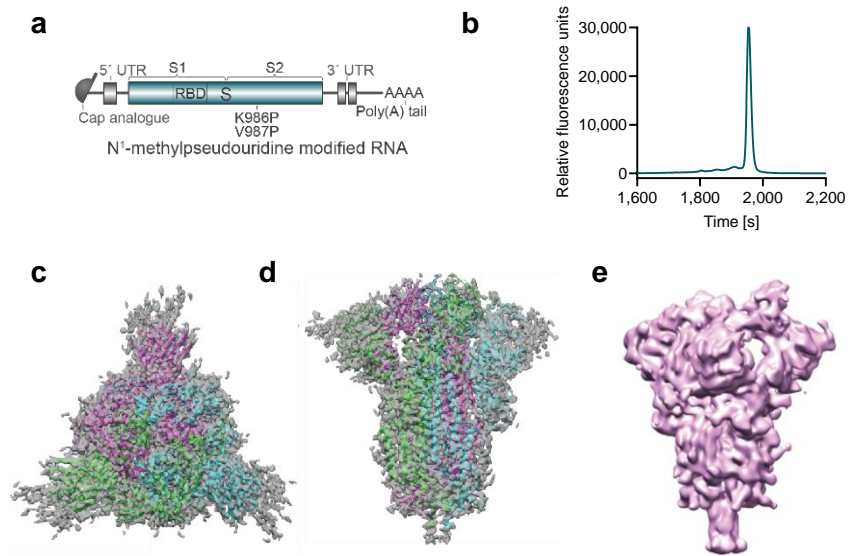


**Figure 1. Vaccine design and characterisation of the expressed antigen.**

**a**, BNT162b2 RNA structure. UTR, untranslated region; S, SARS-CoV-2 S glycoprotein; S1, N-terminal furin cleavage fragment; S2, C-terminal furin cleavage fragment; RBD, receptor-binding domain. Positions of the P2 mutation (K986P and V897P) are indicated. **b**, Liquid capillary electropherogram of *in vitro* transcribed BNT162b2 RNA. **c**, A 3.29 Å cryoEM map of P2 S, with fitted and refined atomic model, viewed down the three-fold axis toward the membrane. **d**, Cryo-EM map and model of (d) viewed perpendicular to the three-fold axis. **e**, Mass density map of TwinStrep-tagged P2 S produced by 3D classification of images extracted from cryo-EM micrographs with no symmetry averaging. This class, in the one-RBD ‘up’, two RBD ‘down’ positioning, represents 20.4% of the population.

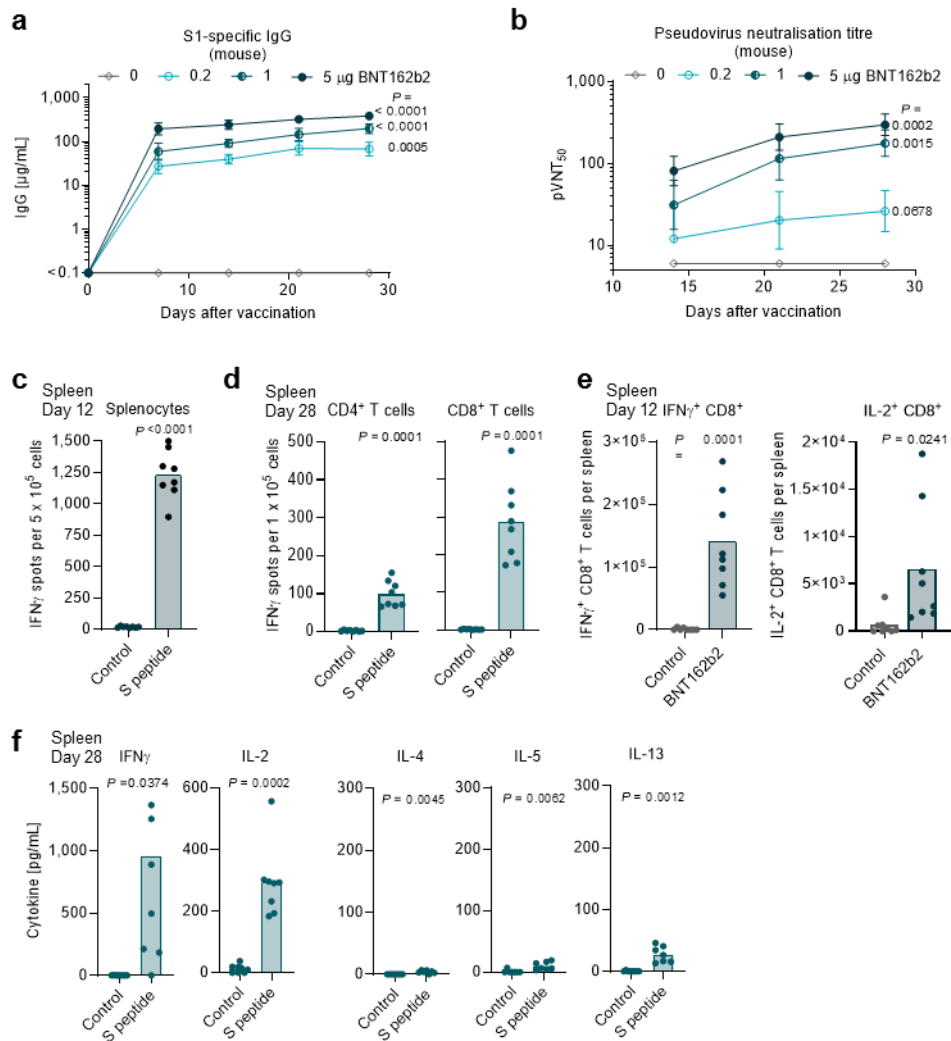


## Figure 2. Mouse immunogenicity.

BALB/c mice (n=8 per group unless otherwise specified) were immunised intramuscularly (IM) with a single dose of with 0.2, 1 or 5 µg BNT162b2 or buffer. Geometric mean of each group ± 95% CI, P-values compare Day 28 to non-immunised (0 µg; n=8) baseline sera (multiple comparison of mixed-effect analysis using Dunnett's multiple comparisons test) (a, b). **a**, S1-binding IgG responses in sera obtained 7, 14, 21 and 28 days after immunisation with 0, 0.2, 1, or 5 µg BNT162b2, determined by ELISA. For day 0 values, a pre-screening of randomly selected animals was performed (n=4). **b**, VSV-SARS-CoV-2 pseudovirus 50% serum neutralising titers (pVNT<sub>50</sub>) of sera from (a). **c-f**, Splenocytes of BALB/c mice immunised IM with BNT162b2 or buffer (control) were *ex vivo* re-stimulated with full-length S peptide mix or negative controls ([c], [e], [f]: no peptide; [d]: irrelevant peptide). Individual values and mean of each group, P-values were determined by a two-tailed paired t-test. **c**, IFN<sub>γ</sub> ELISpot of splenocytes collected 12 days after immunisation with 5 µg BNT162b2. **d**, IFN<sub>γ</sub> ELISpot of isolated splenic CD4<sup>+</sup> or CD8<sup>+</sup> T cells collected



28 days after immunisation with 1  $\mu\text{g}$  BNT162b2. **e**, CD8<sup>+</sup> T-cell specific cytokine release by splenocytes collected 12 days after immunisation with 5  $\mu\text{g}$  BNT162b2 or buffer (Control), determined by flow cytometry. S-peptide specific responses are corrected for background (no peptide). **f**, Cytokine production by splenocytes collected 28 days after immunisation with 1  $\mu\text{g}$  BNT162b2, determined by bead-based multiplex analysis (n=7 for IL-4, IL-5 and IL-13, one outlier removed via routs test [Q=1%] for the S peptide stimulated samples).

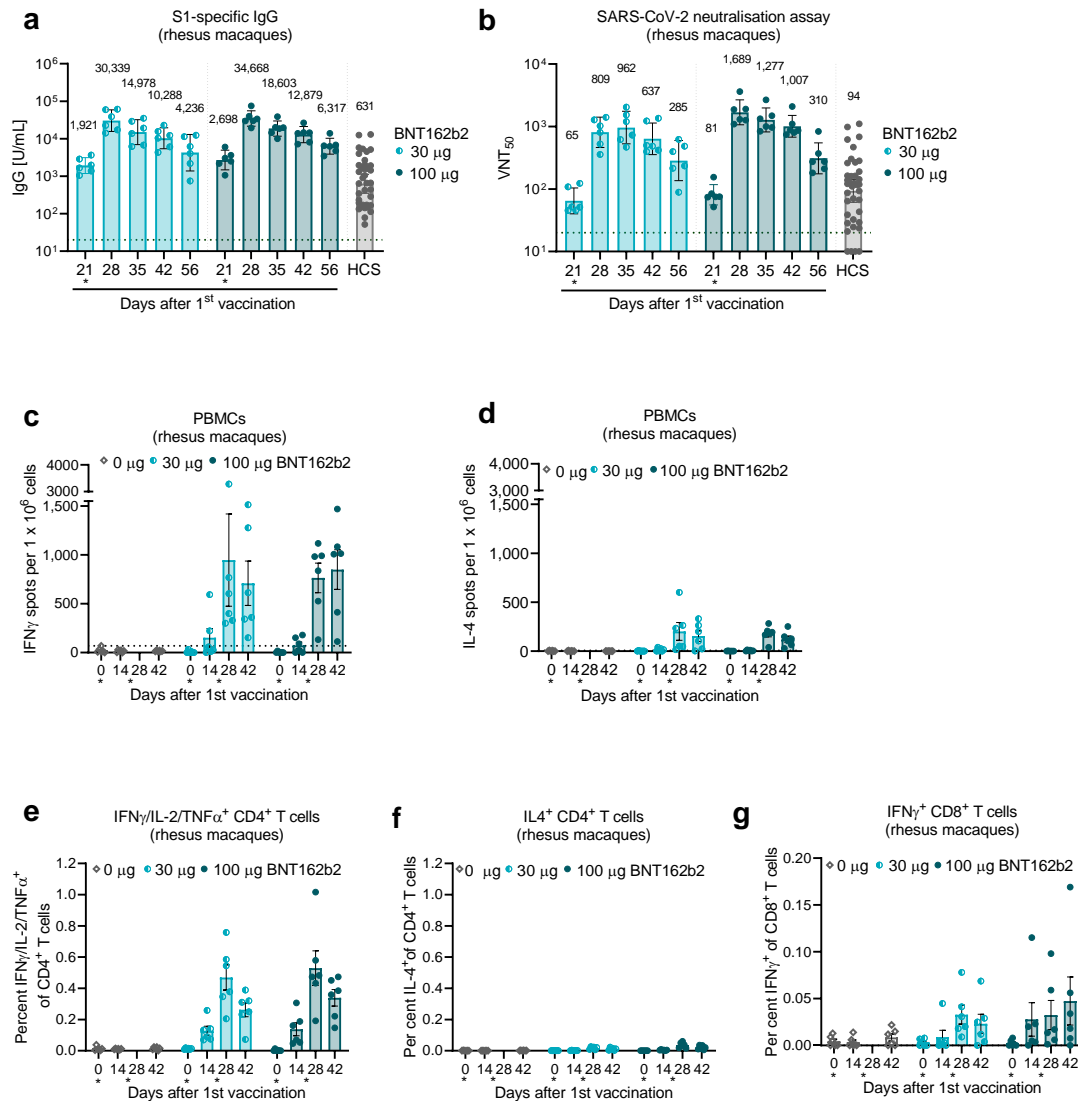


### Figure 3. Rhesus macaque immunogenicity.

Rhesus macaques (n=6 per group) were immunised on Days 0 and 21 with 30 µg or 100 µg BNT162b2 or buffer. Sera and PBMCs were collected at the times indicated. Human convalescent sera (HCS) were obtained from SARS-CoV-2-infected patients at least 14 days after PCR-confirmed diagnosis and at a time when acute COVID-19 symptoms had resolved (n=38). **a**, Concentration, in arbitrary units, of IgG binding recombinant SARS-CoV-2 S1. **b**, SARS-CoV-2 50% virus neutralisation titers (VNT<sub>50</sub>). **c-g**, PBMCs collected on Day 42 were *ex vivo* re-stimulated with full-length S peptide mix. **c**, IFN<sub>γ</sub>, and **d**, IL-4 ELISpot. **e**, **f**, CD4<sup>+</sup> T-cell specific, and **g**, CD8<sup>+</sup> T-cell specific cytokine release, determined by flow cytometry. Heights of bars indicate the geometric (a-b) or arithmetic (c-g) means for each group. Whiskers indicate 95% confidence intervals (CI's; a-b) or standard errors of means (SEMs; c-g). Every symbol represents one animal. Horizontal dotted lines mark the LLODs. Values below the LLOD set to ½ the LLOD. Asterisks below the x-axis indicate the day of Dose 2.

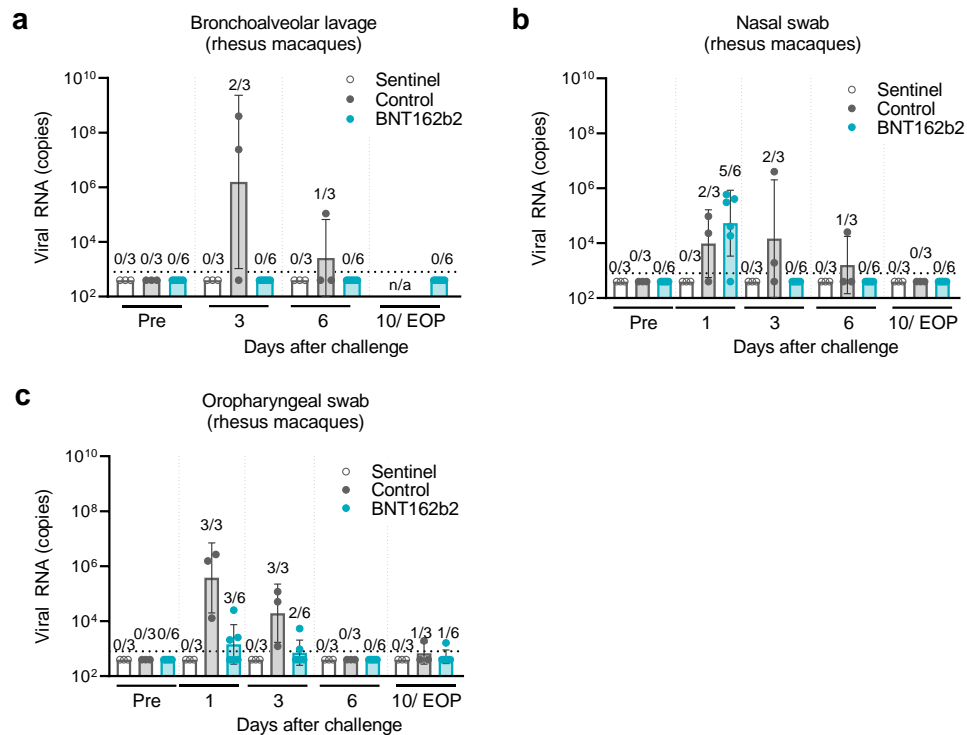
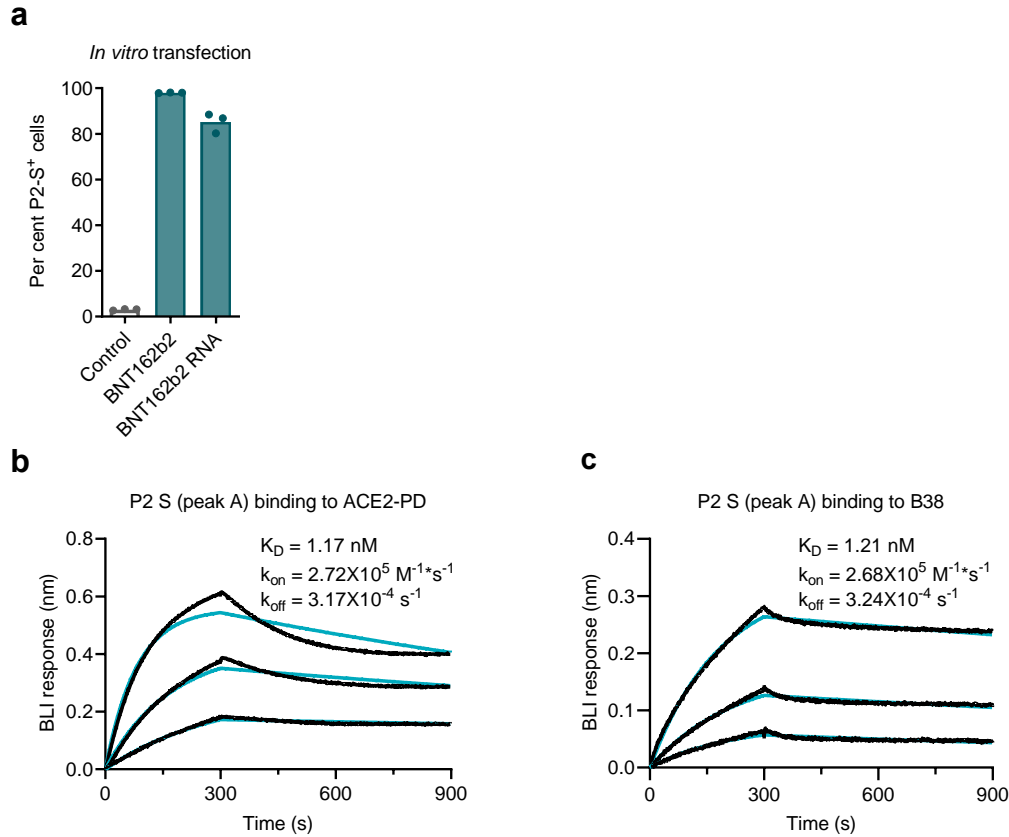


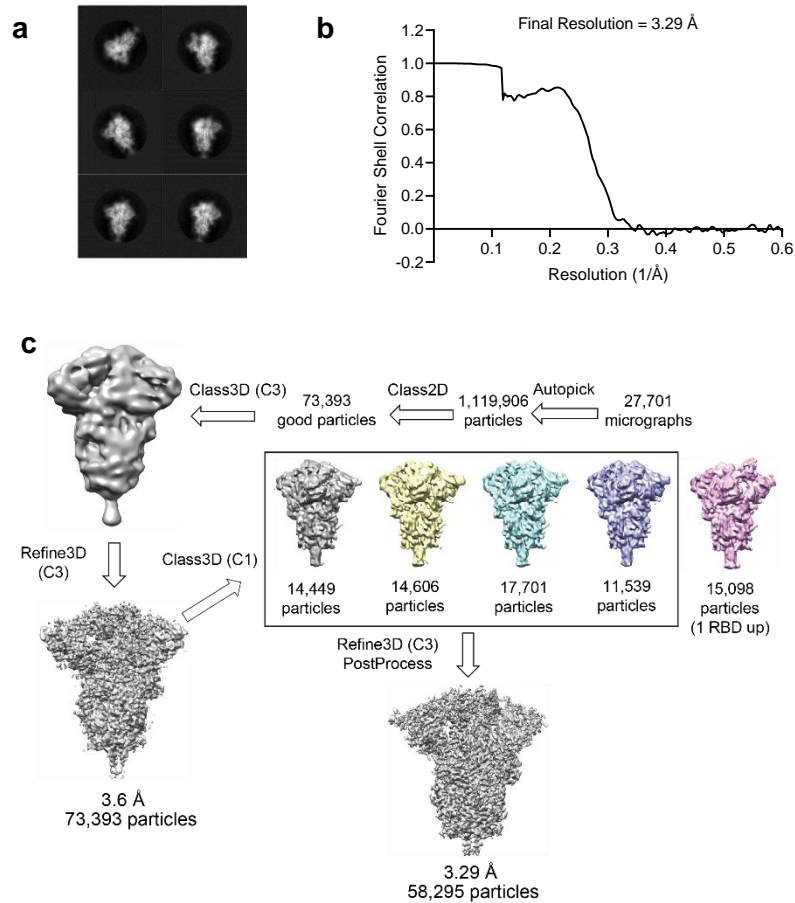
#### Figure 4. Protection of rhesus macaques from challenge with infectious SARS-CoV-2.

Fifty-five days after the Dose 2 of 100  $\mu$ g BNT162b2 (n=6) or saline control (n=3), rhesus macaques were challenged with  $1.05 \times 10^6$  total pfu of SARS-CoV-2 split equally between the IN and IT routes. Non-immunised rhesus macaques (n=3) were mock-challenged with cell culture medium (sentinel). Viral RNA levels were detected by RT-qPCR. BAL was performed and nasal and oropharyngeal (OP) swabs obtained at the indicated time points. Final collection of samples was on Day 10 relative to challenge for the sentinel and control groups and at the end of protocol (EOP) on Day 7 or 8 for the BNT162b2-immunised group. Ratios above data points indicate the number of viral RNA positive animals among all animals per group. Heights of bars indicate geometric means. Whiskers indicate geometric standard deviations. Every symbol represents one animal. Dotted lines indicate the lower limits of detection (LLOD). Values below the LLOD were set to  $\frac{1}{2}$  the LLOD. **a**, Viral RNA in bronchoalveolar lavage (BAL) fluid. **b**, Viral RNA in nasal swabs. **c**, Viral RNA in OP swabs. The statistical significance by a non-parametric test (Friedman's test) of differences in viral RNA detection between control-immunised and BNT162b2-immunised animals after challenge was  $p=0.0014$  for BAL fluid,  $p=0.2622$  for nasal swabs, and  $p=0.0007$  for OP swabs. n/a – not available.

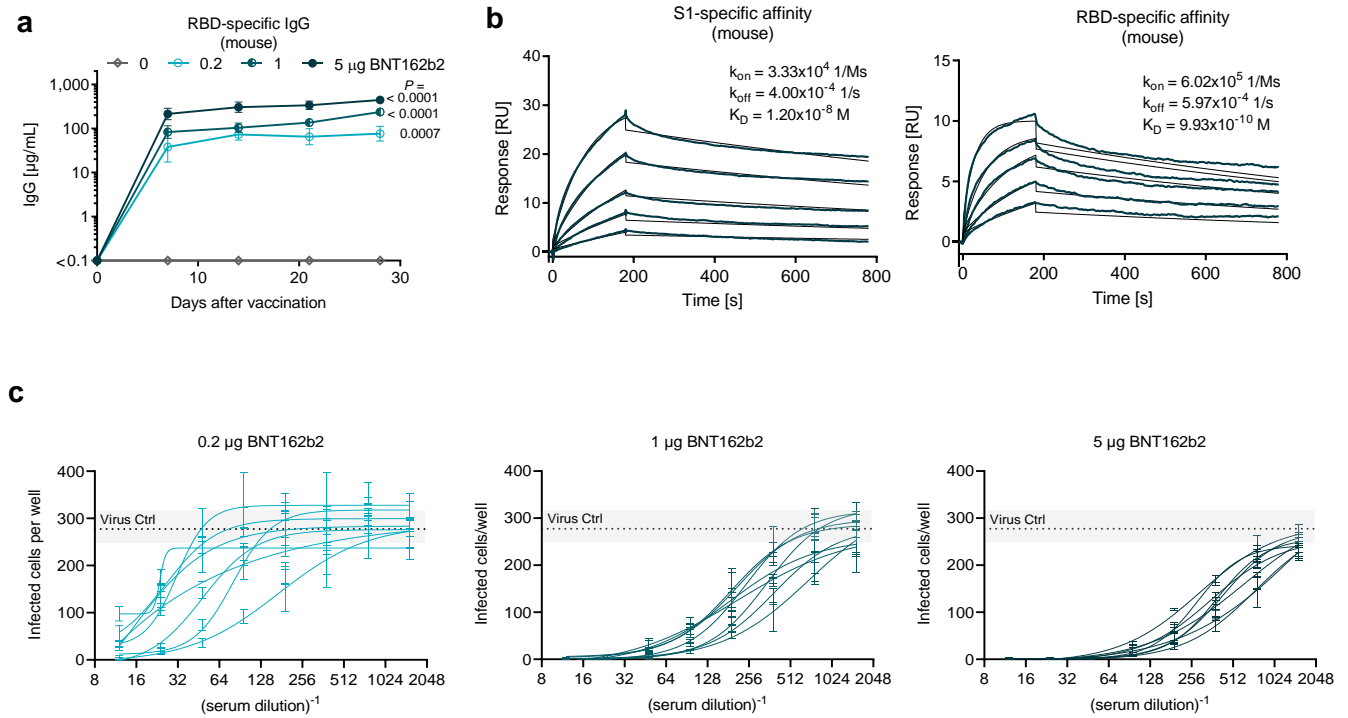


### Extended Data Figure 1. P2 S expression and receptor affinity.

**a**, Fraction of HEK293T/17 cells expressing P2 S determined by flow cytometry after incubation with BNT162b2 RNA formulated as LNP (BNT162b2), BNT162b2 RNA formulated with a transfection reagent (BNT162b2 RNA), or no RNA (Control), determined by flow cytometry. **b**, **c**, P2 S with a C-terminal TwinStrep tag, expressed in Expi293F cells, was detergent solubilized and purified by affinity and size exclusion chromatography. Protein from the first peak of a size exclusion column, containing intact P2 S and dissociated S1 and S2 fragments, was assayed by biolayer interferometry. Sensorgram of the binding kinetics of TwinStrep-tagged P2 S to immobilised **b**, human ACE2-PD and **c**, B38 monoclonal antibody.

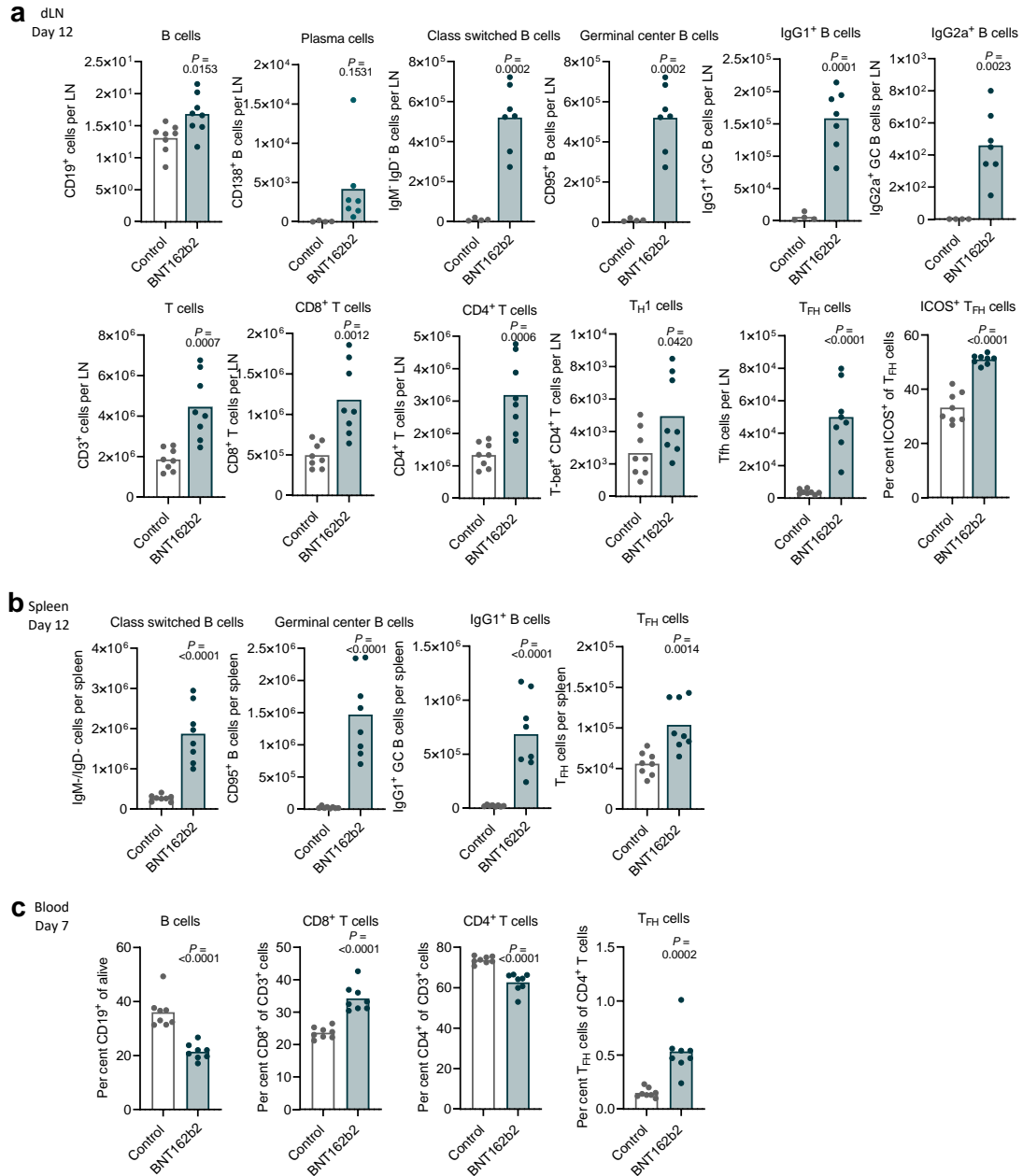


**Extended Data Figure 2. Structure analysis of BNT162b2-encoded P2 S by cryo-electron microscopy**  
**a**, 2D class averages of TwinStrep-tagged P2 S particles extracted from cryo-EM micrographs.. Box edge: 39.2 nm in each dimension. **b**, Fourier shell correlation curve from RELION gold-standard refinement of the P2 S trimer. **c**, Flowchart for cryo-EM data processing of the complex.



### Extended Data Figure 3. BNT162b2-elicited antibody responses in mice.

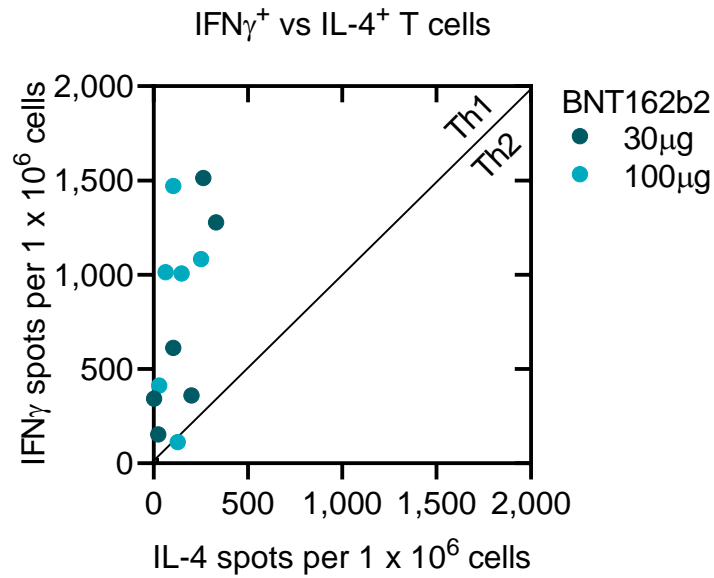
BALB/c mice (n=8 per group) were immunised intramuscularly (IM) with 0.2, 1 or 5 µg of BNT162b2 or buffer. **a**, RBD-binding IgG responses in sera obtained 7, 14, 21 and 28 days after immunisation, determined by ELISA. For day 0, a pre-screening of randomised animals was performed (n=4). Geometric mean of each group is shown. **b**, Representative surface plasmon resonance sensorgram of the binding kinetics of recombinant S1 (*left*) and RBD (*right*) to immobilised mouse IgG from serum 28 days after immunisation with 5 µg BNT162b2 (n=8). Actual binding (dark blue) and the best fit of the data to a 1:1 binding model (thin line in black). **c**, Number of infected cells per well in pseudovirus neutralisation assays conducted with serially diluted mouse serum samples obtained 28 days after immunisation with BNT162b2 are shown (n=8 per group, see also Figure 2b).



### Extended Data Figure 4. B-cell and T-cell phenotyping in lymph nodes, spleen and blood of BNT162b2 immunised mice.

Mice (n=8 per group) were immunised with 5 µg BNT162b2 or buffer (Control). P-values were determined by an unpaired two-tailed t-test. **a+b**, B-cell and T-cell numbers 12 days after immunisation in (a) draining lymph nodes (dLN; for B-cell subtyping only: n=4 for control, n=7 for BNT162b2 immunised group) or (b) the spleen, determined by flow cytometry. The percentage of ICOS<sup>+</sup> cells among T follicular helper cells (T<sub>FH</sub>) in dLNs is depicted on the lower right in (a). **c**, B- and T-cell fractions in the blood seven days after immunisation.





**Extended Data Figure 5. Scatterplot of IL-4 vs. IFN $\gamma$  ELISpot of S peptide stimulated PBMCs collected on Day 42.**

Rhesus macaques (n=6 per group) were immunised on Days 0 and 21 with 30  $\mu$ g or 100  $\mu$ g BNT162b2 (see Fig. 3c,d) and individual animal values are shown.

## Extended Data Table 1. Electron cryomicroscopy data collection, 3D reconstruction and refinement statistics.

<b>Data collection</b>		
EM equipment	Titan Krios (Thermo Fisher Scientific)	
Voltage (keV)	300	
Detector	K2 Summit	
Energy filter	Gatan GIF, 20 eV slit	
Nominal Magnification	165,000 x	
Pixel size (Å)	0.435 (super-resolution)	
	Grid 1	Grid 2
Electron dose ( $e^-/\text{Å}^2$ )	50.32	50.12
Dose rate ( $e^-/\text{Å}^2/\text{sec}$ )	8.4	8.33
Defocus range ( $\mu\text{m}$ )	-1.2 to -3.4	-1.2 to -3.4
Number of collected micrographs	10422	17279
<b>3D Reconstruction</b>		
Software	Warp, Relion	
Number of used particles		
Symmetry imposed	C3	
Global Resolution (Å)		
FSC 0.143	3.29	
Applied B factor ( $\text{Å}^2$ )	-50	
<b>Refinement</b>		
Software	Phenix, Coot	
Protein residues	22,051	
Map Correlation Coefficient	0.82	
RMSD		
Bond length (Å)	0.011	
Bond angles (°)	0.962	
Ramachandran plot statistics (%):		
Preferred	90.4	
Allowed	9.59	
Outlier	0	
Poor Rotamers (%)	11.06	
MolProbity Score	2.96	
Clashscore (all atoms)	13.23	